Available online at www.sciencedirect.com
ScienceDirect
Lithos 96 (2007) 415–435
LITHOS
www.elsevier.com/locate/lithos

Neo-Proterozoic rift-related syenites (Northern Damara Belt, Namibia): Geochemical and Nd–Sr–Pb–O isotope constraints for mantle sources and petrogenesis

S. Jung [a,b,*], E. Hoffer [a], S. Hoernes [c]

[a] *Philipps-Universität Marburg, Fachbereich Geowissenschaften, Lahnberge/Hans-Meerwein-Straße, 35032 Marburg, FRG*
[b] *Max-Planck-Institut für Chemie, Abt. Geochemie, Postfach 3060, 55020 Mainz, FRG*
[c] *Mineralogisch-Petrologisches Institut der Universität Bonn, Poppelsdorfer Schloß, 53115 Bonn, FRG*

Received 7 July 2005; accepted 15 November 2006
Available online 29 December 2006

Abstract

Major element, trace element and Nd–Sr–Pb–O isotope data for a suite of Neo-Proterozic, pre-orogenic, rift-related syenites from the Northern Damara orogen (Namibia) constrain their sources and petrogenesis. New U–Pb ages obtained on euhdreal titanite of inferred magmatic origin constrain the age of intrusion of the Lofdal and Oas syenites to ca. 750 Ma compatible with previous high-precision zircon analyses from the Oas complex. Major rock types from Lofdal and Oas are mildly sodic nepheline-normative and quartz-normative syenites and were primarily generated by fractional crystallization from a mantle-derived alkaline magma. Primitive samples from Lofdal and Oas show depletion of Rb, K and Th relative to Ba and Nb together with variable negative anomalies of P and Ti on a primitive mantle-normalized diagram. Evolved samples from Oas develop significant negative Ba, Sr, P and Ti anomalies and positive U and Th anomalies mainly as a function of crystal fractionation processes. The lack of a pronounced negative Nb anomaly in samples from Lofdal suggests that involvement of a crustal component is negligible. For the nepheline-normative samples from Lofdal, the unradiogenic Sr and radiogenic Nd isotope composition and low $\delta^{18}O$ values suggest derivation of these samples from a moderately depleted lithospheric upper mantle with crustal-like U/Pb ratios ($^{87}Sr/^{86}Sr$: 0.7031–0.7035, ε Nd: ca. +1, $\delta^{18}O$: 7‰, $^{206}Pb/^{204}Pb$: ca.18.00, $^{207}Pb/^{204}Pb$: 15.58–15.60). Primitive samples of the Oas quartz-normative syenites have identical isotope characteristics ($^{87}Sr/^{86}Sr$: 0.7034, ε Nd: ca. +1, $\delta^{18}O$: 6.5‰, $^{206}Pb/^{204}Pb$: ca.18.00, $^{207}Pb/^{204}Pb$: 15.59) whereas more differentiated samples have higher $^{87}Sr/^{86}Sr$ ratios (0.709–0.714), slightly higher $\delta^{18}O$ values (7.0–7.1‰), less radiogenic ε Nd values (−1.1 to −1.4) and more radiogenic $^{206}Pb/^{204}Pb$ ratios up to 18.27. These features together with model calculations using Sr–Nd–Pb isotopes suggest modification of a primary syenite magma by combined AFC processes involving ancient continental crust. In this case, high Nb abundances of the parental syenite liquid prevent the development of significant negative Nb anomalies that may be expected due to interaction with continental crust.
© 2006 Elsevier B.V. All rights reserved.

Keywords: Pan-African alkaline magmatism; Syenites; Trace elements; Sr–Nd–Pb–O isotopes; Damara orogen; Namibia

* Corresponding author. Philipps-Universität Marburg, Fachbereich Geowissenschaften, Lahnberge/Hans-Meerwein-Straße, 35032 Marburg, FRG. Fax: +49 6421 2828919.
E-mail address: jungs@staff.uni-marburg.de (S. Jung).

0024-4937/$ - see front matter © 2006 Elsevier B.V. All rights reserved.
doi:10.1016/j.lithos.2006.11.005

1. Introduction

Alkaline igneous rocks are widely distributed in space and time and occur in almost all tectonic settings although they are volumetrically insignificant rock types. Their occurrence seems to be rare in the Archaean and Early Proterozoic compared with the Late Proterozoic and Phanerozoic (e.g., Blichert-Toft et al., 1996). Generally, they may be grouped into three categories: those formed in continental rift valleys or divergent

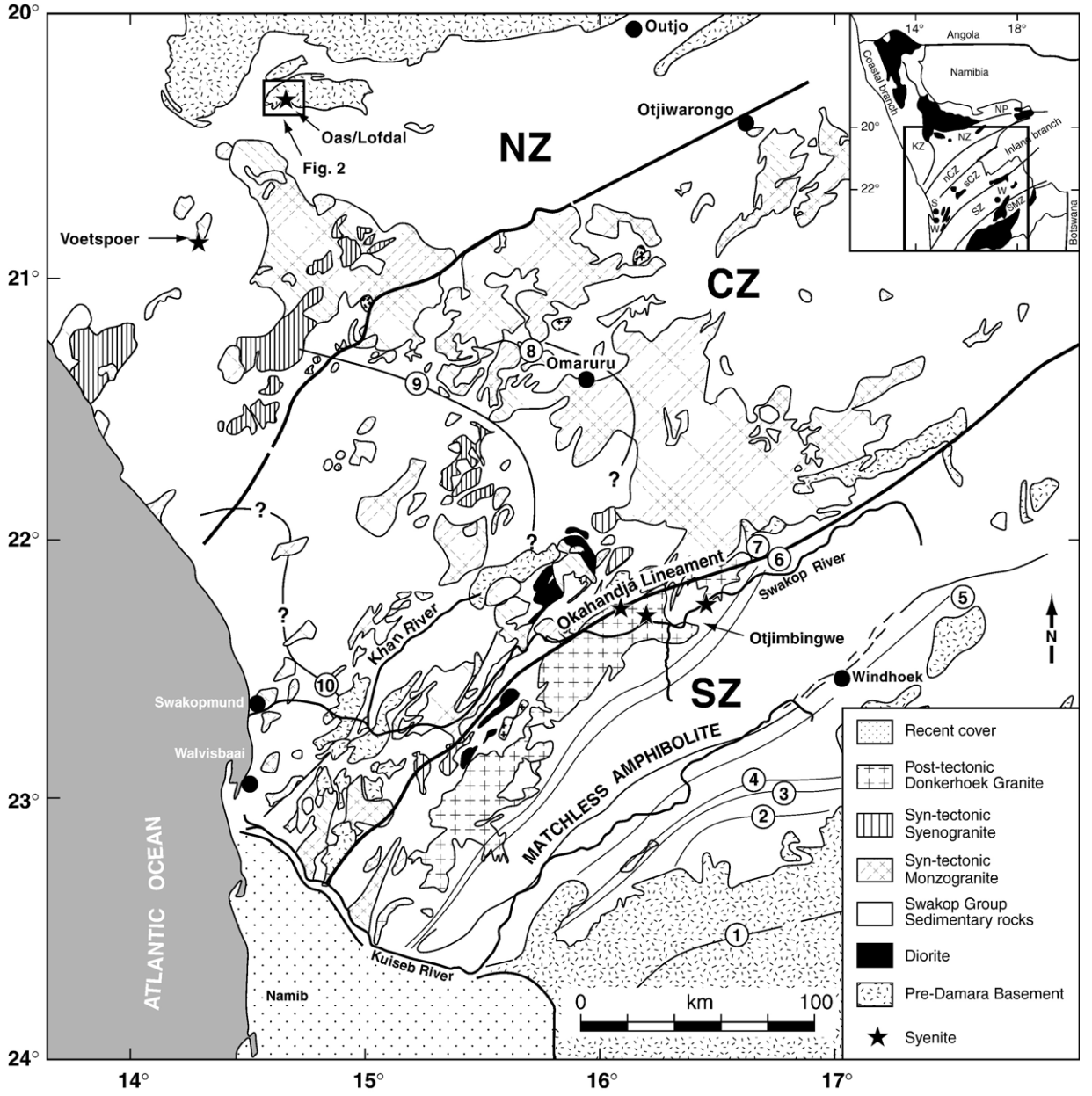

Fig. 1. Generalized geological map showing the study area within the Northern Zone of the Damara orogen, Namibia. Abbreviations in inset: KZ: Kaoko Zone, NP: Northern Platform, NZ: Northern Zone, nCZ: northern central Zone, sCZ: southern Central Zone, SZ: Southern Zone, SMZ: Southern Margin Zone, W: Walvisbay, S: Swakopmund, Wh: Windhoek. Also shown are the syn-orogenic syenite occurrences at Voetspoer and Otjimbingwe. Isograd map (Hartmann et al., 1983) gives the distribution of regional metamorphic isograds within the southern and central Damara orogen. Isograds: (1) biotite-in, (2) garnet-in, (3) staurolite-in, (4) kyanite-in, (5) cordierite-in, (6) andalusite ↔ sillimanite, (7) sillimanite-in according to staurolite-breakdown, (8) partial melting due to: muscovite + plagioclase + quartz + H_2O ↔ melt + sillimanite, (9) K-feldspar + cordierite-in, (10) partial melting due to: biotite + K-feldspar + plagioclase + quartz + cordierite ↔ melt + garnet.

continental margins, those formed in oceanic and continental intraplate setting without clear tectonic control and those associated with subduction zone magmatism (e.g., Fitton and Upton, 1987). Alkaline rocks in general can be derived either from partial melting of metasomatized LREE (Light Rare Earth) and LILE (Large-Ion-Lithophile-Elements) enriched upper mantle sources (Dawson, 1987), from unmetasomatized asthenospheric mantle by very small degrees of melting followed by extensive crystal fractionation (e.g., Fitton, 1987) or from the interaction of asthenosphere-derived melts with the overlying lithosphere (e.g., Menzies, 1987). Specific models for the generation of syenites include crystal fractionation from alkali basaltic precursors combined with varying degrees of crustal contamination (Ewart, 1982; Brown and Becker, 1986; Fitton, 1987; Downes, 1987; Thirlwall and Burnard, 1990; Fowler, 1992; Foland et al., 1993; Brotzu et al., 1997; Smith et al., 1997; Mingram et al., 2000; Litvinovsky et al., 2002) or small-degree partial melting of enriched upper mantle (Sutcliff et al., 1990) or even lower crust (Harris et al., 1983; Smith et al., 1988; Gleason et al., 1994; Lubala et al., 1994; Zanvilevich et al., 1995). Additionally, magma mixing processes with subsequent differentiation of the hybrid liquids can be important (Zhao et al., 1995; Litvinovsky et al., 1999). Lastly, mixing of mantle-derived silica-undersaturated alkaline magmas with granitic magmas formed by melting of lower crustal material above a zone of mafic underplating is also a viable process to explain the common coeval occurrence of silica-undersaturated and oversaturated syenites.

In the Proterozoic to Phanerozoic Damara orogen of Namibia, pre-orogenic to syn-orogenic syenites have been reported from a number of localities. These include (from north to south and also from oldest to youngest) the (i) pre-orogenic, rift-related Oas and Lofdal syenites, (ii) the syn-orogenic Voetspoer syenite and (iii) the syn-orogenic Otjimbingwe syenite (Fig. 1). Due to a lack of geochemical and high-precision isotope data the origin and tectonic significance of the Oas and Lofdal are so far not well constrained. For the Otjimbingwe and Voetspoer syenites, a complex model involving interaction of distinct lithospheric mantle domains with crustal material has been proposed (Jung et al., 2004, 2005). One difficulty in evaluating models for the petrogenesis of syenites is the lack of data that place limits on the relative importance of different components (lower crust, upper crust, mantle) involved in syenite formation. Rare Earth Element (REE) abundances, whole rock Nd, Sr and O isotopes and Pb isotopes from leached feldspars are well suited for this purpose. Based on such a data set, a detailed geochronological and isotopic study of the Neoproterozoic Oas and Lofdal syenites is presented. The results are used to constrain the effects of crustal contamination in the genesis of coeval nepheline-normative and quartz-normative syenites and to infer the nature of their sources.

2. Analytical techniques

Whole rock powders were prepared using a jaw crusher, a ball mill and an agate mortar. Major and some trace elements (except for REE) were determined on fused lithium-tetraborate glass beads using standard XRF techniques at the University of Bonn. Rare earth elements were either analyzed by ICP-AES techniques at the University of Marburg following separation of the matrix elements by ion exchange (Heinrichs and Herrmann, 1990) or by ICP-MS techniques at GFZ Potsdam (Dulski, 2001). Accuracy and precision were monitored by repeated measurements of international standards and in-house standards calibrated against international rock standards (Jung et al., 2003). Loss on ignition (LOI) was determined gravimetrically after heating the samples at 1050 °C for 1 h (Lechler and Desilets, 1987). FeO was measured titrimetrically with standard techniques. Accuracy was controlled by repeated measurements against several international and in-house standards.

For the Rb–Sr and Sm–Nd whole rock isotope analyses the samples were spiked with a $^{149}Sm/^{150}Nd$ and a $^{85}Rb/^{84}Sr$ tracer and digested in concentrated HF-HNO_3 in 3 ml screw-top Teflon® vials inside Krogh-style Teflon® bombs at 200 °C for 3 days. After complete dissolution the samples were dried down and redissolved in 2.5 N HCl. To insure complete dissolution multiple dissolution steps involving 2.5 N HCl and a high acid/sample ratio were performed. Rubidium, Sr and REE were separated using standard cation exchange columns with a DOWEX® AG 50 W-X 12 resin using 2.5 N HCl for Rb and Sr and 6 N HCl for the REE. Neodymium and Sm were separated from the other REE on HDEHP coated Teflon® columns and 0.12 N HCl for Nd and 0.3 N HCl for Sm. Isotope analyses were carried out at the Max-Planck-Institut für Chemie at Mainz with a Finnigan MAT 261 multicollector thermal ionization mass spectrometer operating in static mode. Rubidium, Sm and Nd were run on Re double filaments and Sr was run on W single filaments loaded with TaF_5. Neodymium isotopes were normalized to $^{146}Nd/^{144}Nd = 0.7219$. The total procedural blank for Nd was <40 pg and is negligible. Repeated measurements of the La Jolla Nd standard gave $^{143}Nd/^{144}Nd = 0.511854 \pm 0.000031$ (2 σ; $n = 24$). The

reproducibilitiy of the Sr standard (NBS 987) is $^{87}Sr/^{86}Sr = 0.710218 \pm 0.000029$ (2 σ; $n = 24$) and the fractionation was corrected to $^{86}Sr/^{88}Sr = 0.1194$. Uncertainties in the $^{87}Sr/^{86}Sr$ and $^{143}Nd/^{144}Nd$ are reported in the last two digits. Typical analytical errors in the $^{87}Rb/^{86}Sr$ and $^{147}Sm/^{144}Nd$ ratios are equal or better than 0.5 % and 0.2%, respectively. For common Pb analyses 30–50 mg of high-purity K-feldspar separates were washed in a mixture of 3:1 HCl:HNO_3 over night on a hotplate to remove surface contamination and subsequently rinsed three times with ultrapure water. After this treatment the separates were leached three times in a mixture of concentrated HF/HNO_3 which resulted in a weight loss of ~70–80%. Subsequently, the remaining residual feldspar was dissolved in concentrated HF and after evaporation redissolved in 2.5 N HCl and 0.6 N HBr and loaded on Teflon® columns filled with DOWEX® AG 1×8 anion exchange resin (100–200 mesh) in chloride form (Mattinson, 1986). The Pb was extracted using conventional HBr/HCl techniques and was loaded on Re single filaments using the H_3PO_4-silica gel method (Cameron et al., 1969). Lead analyses were corrected for mass fractionation by a factor of 0.11% per amu. The reproducibility of the standard NBS 982 was estimated to be 0.068%, 0.064% and 0.071% for the $^{206}Pb/^{204}Pb$, $^{207}Pb/^{204}Pb$ and $^{208}Pb/^{204}Pb$ ratio, respectively. The total procedure blank was <100 pg Pb and is therefore negligible.

For U–Pb analyses of titanite, the crushed rocks were sieved through a 40–80 mesh sieve. Subsequently, the titanites were purified by magnetic separation, methylen iodide and then handpicking which produced high-purity separates. Only titanites free of inclusions were used. For each analysis 5–10 mg was used. The titanites were washed in warm deionized water to remove surface contamination and were spiked with a $^{205}Pb/^{233}U$ spike before digesting in concentrated HF/HNO_3 in 3 ml screw-top Teflon® vials inside Krogh-style Teflon bombs at 200 °C for several days. The Pb was separated using HCl–HBr chemistry and the U was separated using Eichrome® resin and an improved 2 N HNO_3/0.02 N HNO_3 chemistry. Lead isotope analyses were carried out as described above for common Pb. In order to correct for initial Pb composition, the Pb composition of leached K-feldspar from each sample was measured and was taken as the initial Pb composition during titanite growth. Uncertainties for the U/Pb and Pb/Pb ratios, ages and corresponding uncertainties were calculated using the programs PBDAT and ISOPLOT (Ludwig, 1991a,b). Total blanks for U were <30 pg and the U analyses were corrected for 0.04% per amu based on repeat analyses of the NBS U 500 standard.

Oxygen isotope analyses were performed at the University of Bonn on ~10 mg aliquots of powdered whole-rock samples, using purified flourine for oxygen extraction (Asprey, 1976), followed by conversion to CO_2 (Clayton and Mayeda, 1963). $^{18}O/^{16}O$ measurements were made on a SIRA-9 triple-collector mass spectrometer manufactured by VG-Isogas. Analytical uncertainties are <0.2‰.

3. Geological setting and rock types

The Damara orogen of Namibia comprises a deeply eroded section of a Pan-African mobile belt that can be divided into a north–south trending coastal branch and a north-east–south-west trending intracontinental branch (see inset to Fig. 1). This mobile belt consists mainly of 1.2 to 2.0 Ga-old basement gneisses, Pan-African plutonic rocks and various metasedimentary rocks. The belt has been divided into several zones based mainly on stratigraphy, metamorphic grade, structure and geochronology (e.g., Miller, 1983). Pre-Damara basement gneisses are overlain by Neoproterozoic metasedimentary sequences, consisting of marble, calcsilicate rocks, quartzite, conglomerate, mica-schists, metamorphosed glaciogenic diamictites, banded iron-stone formations, Al-rich metapelites and migmatites. 560–460 Ma-old granites are the most common igneous rock type (ca. 94%) and crop out over an area of approximately 75,000 km^2. The remaining igneous bodies are equally divided between diorite and tonalite/granodiorite (Miller, 1983).

In the Central Zone, the metamorphic grade increases from east to west reaching high-grade conditions with local partial melting in the coastal area (Hartmann et al., 1983). These high-grade conditions culminated in low-pressure high-temperature granulite-facies conditions with the temperature estimated to have been between 680 °C and 750 °C at 5–6 kbar (Masberg et al., 1992; Bühn et al., 1995; Jung et al., 1998a,b; 2000; Jung and Mezger, 2003). The timing of orogenic events and the age of the peak of metamorphism within the Central Zone of the Damara orogen is constrained by combined U–Pb monazite ages and Sm–Nd garnet-whole rock ages indicating that the time span of high-grade metamorphism ranges from ca. 540 Ma to 470 Ma with an age of ca. 510 Ma for the (main) peak of regional metamorphism (Jung et al., 2000; Jung and Mezger, 2001, 2003).

The northern Zone is characterized by the occurrence of Pre-Damara basement rocks (Welwitschia and Kamanjab inliers) that belongs to the Proterozoic Huab Gneiss domain. These inliers are flanked by

Damaran rocks, comprising the Nosib, Swakop and Mulden group series consisting of pebbly feldspathic quartzites, carbonates and fine clastic sedimentary rocks (Fig. 2). In the area, alkaline and peralkaline rhyolite ash-flow tuffs dominate but other felsic extrusive rocks and mafic to intermediate intrusive rocks also occur. The great thickness of these lavas and tuffs (up to 6 km; Miller, 1983) and their localized occurrence at the northern margin of the orogen seem to indicate that emplacement of these igneous rocks was associated with crustal extension. It is therefore suggested that this igneous activity coincides with continental breakup at the southern margin of the Kongo craton.

Taken together, the Oas and Lofdal syenite complexes form an irregular intrusive body with an inferred dimension of ca. 10×8 km (Fig. 2). Both complexes are distinctly discordant with respect to the country rock gneisses and metasedimentary rocks. The main body of the Oas quartz-normative syenite trends roughly E–W and is intrusive into Pre-Damara basement rocks (the Huab gneiss) and Damaran metasedimentary rocks of the Nosib and Swakop groups. At the western marginal phase of the main body of the Oas quartz-normative syenite contamination effects with the Huab gneiss in the form of disaggregated rafts of quartz–felspar–biotite gneisses are visible. The smaller satellite body of the Oas quartz-normative syenite and the Lofdal nepheline-normative syenite located farther north is trending NE–SW and is intrusive into the Huab gneiss (Fig. 2). The Lofdal nepheline-normative syenite is made up of monotonous, coarse- to medium-grained dark grey to light grey syenite whereas the Oas quartz-normative syenite consists of medium-grained dark grey to brick red syenite. Evidence of thermal effects in the contact

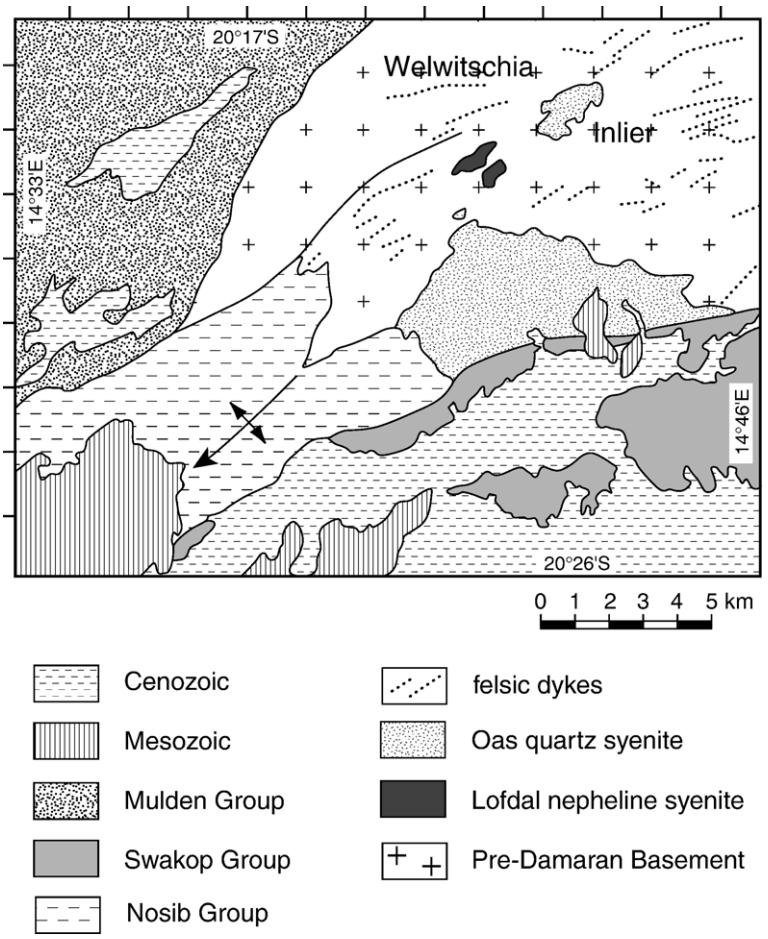

Fig. 2. Detailed map of the Oas/Lofdal area with syenite occurrences. Note the occurrence of the Lofdal nepheline-normative syenites exclusively within the Huab basement (Welwitschia inlier) whereas the Oas quartz-normative syenites crop out within the basement and between basement and Damara metasedimentary strata.

zones to the gneiss or metasedimentary rocks (i.e., decrease in grain size) has not been observed but the presence of vein-like apophyses into the country rocks can be observed in places. Due to the small size of the individual intrusive bodies structural heterogeneities are rarely observed. These heterogeneities are restricted to small-scale banding which most probably resembles layering of contrasting felsic/mafic mineral proportions. Some of these layered felsic/mafic mineral associations form irregularly intercalated light and dark lens-like segregtions that have similar magmatic textures than the main body and lack signs of recrystallization and tectonic deformation.

4. Petrography

Samples from Oas quartz-normative syenite and Lofdal nepheline-normative syenite are texturally homogeneous and undeformed. Samples from Lofdal contain large euhedral nepheline, perthitic alkali feldspar and bright-green alkali amphibole beside minor amounts of plagioclase. More evolved samples, especially those from Oas contain brown amphibole and additionally interstitial quartz. Some K-feldspar phenocrysts display a concentric zoning of Ab-rich and Or-rich compositions. Large grains may show twinning according to the Carlsbad law and in some samples, K-feldspar shows concentric arrangement of small grains of titanite and apatite. In both suites, subhedral, late-stage amphibole is usually associated with and often rimmed by dark brown biotite and late-stage albite is common in these rocks. Accessory minerals include euhedral titanite, apatite, titanomagnetite, and zircon in decreasing order of abundance. Alteration (i.e., crystallization of late-stage muscovite) is common and affects mostly nepheline, alkalifeldspar and amphibole.

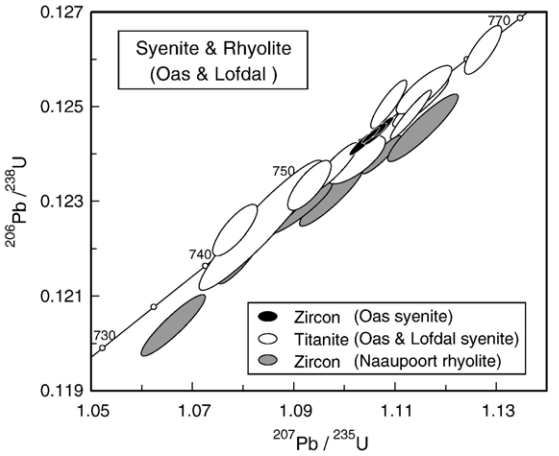

Fig. 3. U–Pb concordia diagram showing titanite analyses from Lofdal and Oas syenites. Also shown are zircon data obtained on Oas syenites and Naaupoort rhyolites from Hoffman et al. (1996).

5. Geochronology

Previous geochronological work yielded in part conflicting results. Hawkesworth et al. (1983) presented a 12 point Rb–Sr whole rock isochron with an age of 764±60 Ma for the Lofdal nepheline-normative syenite whereas the nearby Oas quartz-normative syenite yielded Rb–Sr whole rock ages of 840±13 and 652±11 Ma which were interpreted as intrusive and metamorphic ages, respectively (Kröner, 1982). Furthermore, Tegtmeyer and Kröner (1985) presented a lower U–Pb intercept age for the Oas quartz-normative syenite

Table 1
U–Pb titanite data from the Lofdal and Oas syenites (northern Damara orogen, Namibia)

Locality	Lofdal	Lofdal	Lofdal	Lofdal	Lofdal	Oas	Oas	Oas	Oas	Oas
Sample	98.1.23	98.1.24	98.1.25	98.1.26	98.1.32	98.1.33	98.1.34	98.1.35	98.1.36	98.1.37
U (ppm)	9.097	9.060	8.753	9.394	9.262	9.345	9.343	8.957	8.935	8.996
Pb (ppm)	1.931	2.148	1.797	2.045	1.808	1.952	2.273	1.899	2.140	1.844
$^{206}Pb/^{204}Pb$	163.7	118.0	183.1	148.8	230.2	169.4	108.3	153.8	118.1	200.3
$^{208}Pb/^{206}Pb$	0.4405	0.4159	0.4106	0.4284	0.4114	0.4620	0.4132	0.4348	0.4293	0.4269
$^{207}Pb/^{206}Pb$	0.06353	0.06321	0.06407	0.06359	0.06428	0.06387	0.06448	0.06411	0.06449	0.06410
Error	0.00016	0.00023	0.00016	0.00018	0.00013	0.00016	0.00025	0.00020	0.00023	0.00013
$^{207}Pb/^{235}U$	1.07972	1.08918	1.10234	1.08440	1.10871	1.06663	1.10204	1.07215	1.11544	1.11572
Error	0.00348	0.00452	0.00329	0.00367	0.00294	0.00355	0.00474	0.00986	0.00447	0.00295
$^{206}Pb/^{238}U$	0.12327	0.12497	0.12479	0.12367	0.12509	0.12112	0.12397	0.12129	0.12544	0.12625
Error	0.00043	0.00042	0.00042	0.00042	0.00042	0.00043	0.00042	0.00111	0.00042	0.00042
$^{206}Pb/^{238}U$ age (m.y.)	749	759	758	752	760	737	753	738	762	766
$^{207}Pb/^{235}U$ age (m.y.)	743	748	754	746	758	737	754	740	761	761
$^{207}Pb/^{206}Pb$ age (m.y.)	726	715	744	728	751	737	757	745	758	745

For analytical details see text.

Table 2
Major and trace element and normative composition from Oas and Lofdal syenites (Northern Damara orogen. Namibia)

	Lofdal	Lofdal	Lofdal	Lofdal	Lofdal	Lofdal	Lofdal	Lofdal	Lofdal	Lofdal	Oas	Oas	Oas	Oas	Oas	Oas	Oas	Oas	Oas	Oas	Oas
	98/1.24	98/1.23	98/1.26	98/1.25	98/1.32	04/1.1	04/1.2	04/1.3	04/1.4	04/1.5	KD 176	KD 177	KD 178	98/1.33	98/1.37	98/1.36	98/1.34	KD 182	KD 184	KD 185	98/1.35
SiO_2	47.83	48.24	48.59	48.70	49.17	49.55	49.96	49.65	47.93	49.19	60.24	60.30	61.41	61.01	61.89	62.43	63.25	64.02	64.80	64.80	64.57
TiO_2	1.13	1.02	1.07	1.05	0.94	0.98	1.19	0.95	1.02	0.82	1.12	1.17	0.96	0.76	0.86	0.30	0.94	0.68	0.35	0.55	0.12
Al_2O_3	19.95	20.13	20.34	20.73	20.43	20.14	20.80	18.78	20.07	19.04	17.49	17.56	17.76	18.10	17.38	18.52	16.84	16.64	16.64	16.71	16.96
Fe_2O_3	5.41	4.25	5.26	4.63	3.65	3.32	2.97	4.93	3.89	2.97	2.23	2.18	1.98	2.92	2.6	0.89	3.70	1.94	2.41	1.44	2.32
FeO	1.68	2.18	2.76	1.78	2.04	2.58	3.07	0.82	2.47	3.07	2.91	3.25	2.60	2.05	2.5	2.48	1.38	2.93	2.10	2.06	0.71
MnO	0.21	0.20	0.27	0.19	0.15	0.21	0.21	0.26	0.25	0.20	0.13	0.13	0.13	0.11	0.11	0.08	0.11	0.11	0.12	0.09	0.09
MgO	0.76	0.64	0.89	0.94	0.56	0.56	0.87	0.50	0.70	0.44	1.17	1.12	0.83	0.95	0.22	0.43	0.84	0.72	0.18	0.22	0.15
CaO	6.07	5.63	6.04	5.49	4.64	4.47	6.44	3.63	5.97	3.68	2.33	2.65	2.49	1.92	1.76	1.41	1.45	1.96	1.30	1.03	1.09
Na_2O	6.36	7.36	5.17	5.62	7.58	7.94	5.44	9.19	8.14	11.65	6.46	6.94	6.55	6.44	6.51	6.37	5.87	6.30	6.04	6.43	7.54
K_2O	5.38	5.95	5.97	6.00	6.88	6.21	6.03	6.57	5.46	7.25	4.69	4.63	4.67	4.92	4.85	5.60	5.40	4.67	5.40	5.79	3.51
P_2O_5	0.55	0.42	0.52	0.52	0.32	0.24	0.58	0.24	0.43	0.21	0.32	0.36	0.28	0.26	0.08	0.11	0.24	0.14	0.04	0.06	0.04
LOI	4.20	3.26	3.65	3.90	2.58	2.00	3.40	3.65	2.57	2.94	1.00	0.58	0.57	0.97	0.89	1.42	0.39	0.44	0.40	0.75	2.06
Total	99.53	99.28	100.53	99.55	98.94	98.49	100.96	99.26	98.90	99.11	100.09	100.87	100.23	100.41	99.65	100.04	100.41	100.55	99.78	99.93	99.16
Sc	3	2	7	8	3	2	2	11	15	8	6	8	8	5	6	3	7	5	6	4	10
V	76	74	95	83	64	61	65	22	76	12	24	28	26	13	15	4	16	42	6	4	14
Cr	5	17	9	6	5	9	5	13	5	5	n.d.	n.d.	n.d.	5	5	5	5	n.d.	n.d.	n.d.	5
Co	7	11	14	11	12	14	3	8	7	3	13	13	13	3	9	4	8	14	14	3	2
Ni	4	9	4	4	4	4	4	4	4	4	n.d.	n.d.	n.d.	4	4	4	4	n.d.	n.d.	n.d.	4
Zn	91	81	115	80	82	77	76	180	89	133	137	138	132	99	120	81	35	102	89	93	65
Ga	19	25	26	27	27	17	26	31	18	33	25	27	27	22	32	21	34	32	28	39	35
Rb	130	150	170	139	181	182	135	196	135	168	132	103	132	116	93	123	28	122	93	160	61
Sr	1655	1142	1311	1356	1233	1377	1214	1778	1266	863	609	663	683	422	146	237	146	104	51	102	83
Y	27	22	16	19	20	15	10	40	19	25	38	36	40	45	45	33	38	65	43	31	43
Zr	558	504	673	476	580	475	439	1170	576	672	436	450	521	455	1001	398	247	1024	1097	201	381
Nb	207	208	226	209	191	183	182	411	255	255	104	150	129	193	214	120	94	185	172	84	84
Ba	2956	2487	2190	2769	2713	2713	2842	1583	2255	2271	1845	1966	1860	1567	520	713	439	303	305	240	509
Pb	5	3	8	7	7	37	8	21	8	35	25	21	19	6	25	21	59	22	13	17	49
Th	2	2	2	2	2	3	2	2	2	2	7	2	5	12	16	12	15	11	19	8	6
U	2	2	2	2	2	2	3	13	2	9	10	7	10	8	9	6	9	5	3	2	7
La	97.1	80.8	59.0	62.4	68.3	51.7	54.6	128.3	84.1	77.5	88.5	67.3	69.6	82.7	101.2	94.0	96.3	119.4	117.8	50.8	69.6
Ce	205	167	132	129	139	110	108	242	169	144	166	130	125	174	232	209	169	236	231	107	134
Nd	74.2	62.5	49.8	48.4	51.4	46.6	43.6	81.0	67.3	47.7	59.4	55.9	49.4	73.1	81.0	72.3	61.6	85.8	79.5	46.4	52.6
Sm	14.3	11.7	10.5	9.0	10.4	7.33	6.97	12.2	10.3	6.80	12.4	9.96	9.60	14.0	13.4	12.8	13.1	15.5	14.7	8.12	10.9
Eu	3.28	2.72	2.13	1.98	2.16	2.09	2.01	3.58	2.91	1.65	3.60	3.42	3.42	3.32	2.48	2.72	2.91	12.86	11.18	13.92	1.21
Gd	8.57	7.09	6.41	5.29	5.88	5.31	5.14	9.87	7.42	4.81	8.02	7.14	7.04	9.91	10.93	9.16	7.41	11.88	9.62	5.92	9.02
Dy	5.45	4.56	4.11	3.85	3.91	3.63	3.62	8.23	5.01	4.03	5.98	5.42	5.62	7.55	9.02	7.14	6.24	10.22	7.18	5.04	8.29
Er	2.27	1.59	1.64	1.45	1.60	1.60	1.65	4.24	2.27	2.37	2.84	2.44	3.44	3.39	4.98	2.63	3.20	5.78	3.52	2.16	4.60
Yb	2.03	1.11	1.46	1.30	1.32	1.74	1.64	3.67	2.43	2.39	2.42	2.12	2.54	2.95	5.47	2.57	2.85	5.3	3.96	2.2	5.55
Lu	0.29	0.15	0.22	0.19	0.20	0.32	0.29	0.54	0.43	0.34	0.40	0.34	0.36	0.45	0.72	0.42	0.40	0.76	0.64	0.36	0.87
Q	0.00	0.00	0.00	0.00	0.00	0.0	0.0	0.0	0.0	0.0	0.00	0.00	0.00	0.19	1.96	0.00	5.18	4.50	6.20	3.13	5.05
Or	31.79	35.16	35.82	35.64	40.66	38.2	37.8	34.2	33.5	32.3	27.72	27.36	27.60	29.08	28.66	33.09	31.91	27.60	31.91	34.22	20.74
Ab	12.84	8.44	12.64	13.90	5.42	10.3	18.2	5.0 (lc)	8.8	3.6	54.26	52.14	55.42	54.49	55.09	53.90	49.61	53.31	51.11	53.72	63.80
An	10.00	4.32	11.39	13.62	1.40	1.0	15.4	0.0	2.2	0.0	4.88	3.09	5.27	5.95	3.88	5.40	3.65	3.33	2.34	0.00	2.07
Ne	22.20	29.16	16.85	18.23	31.81	32.3	16.6	34.0	34.0	40.8	0.22	3.57	0.00	0.00	0.00	0.00	0.00	0.00	0.00	0.00	0.00
Di	4.08	3.44	4.78	3.44	3.01	4.6	3.7	6.6	4.1	6.8	3.75	6.35	4.33	1.48	3.49	0.75	1.53	4.60	3.30	4.07	0.81
Hy	0.00	0.00	0.00	0.00	0.00	0.0	0.0	0.0	0.0	0.0	0.00	0.00	1.62	1.97	0.00	0.88	1.38	2.34	0.26	0.48	0.00
Ol	0.00	0.00	0.00	0.00	0.00	0.0	1.3	0.0	0.0	0.0	2.17	1.57	0.08	0.00	0.00	2.48	0.00	0.00	0.00	0.00	0.00
wo	4.71	6.87	4.09	3.24	6.54	6.2	0.0	5.7	8.6	3.1	0.00	0.00	0.00	0.00	0.09	0.00	0.00	0.00	0.00	0.00	0.85
Il	2.15	1.94	2.03	1.99	1.79	1.9	2.0	1.9	2.8	1.6	2.13	2.22	1.82	1.44	1.63	0.57	1.79	1.29	0.66	1.04	0.23
mag	2.82	4.72	6.68	3.31	4.34	5.0	4.6	0.0	5.9	0.0	3.23	3.16	2.87	4.23	3.77	1.29	2.08	2.81	3.49	1.78	2.23
hem	3.46	0.99	0.66	2.34	0.66	0.0	0.0	0.0	0.0	0.0	0.00	0.00	0.00	0.00	0.00	0.00	2.26	0.00	0.00	0.00	0.78
Ti	0.00	0.00	0.00	0.00	0.00	0.0	0.0	0.0	0.0	0.0	0.00	0.00	0.00	0.00	0.00	0.00	0.00	0.00	0.00	0.00	0.00
ap	1.27	0.97	0.74	0.51	0.74	0.6	0.5	0.6	1.0	0.5	0.74	0.83	0.65	0.60	0.19	0.25	0.56	0.32	0.09	0.14	0.09

LOI: loss on ignition. Major elements in wt.%. Trace elements in ppm.

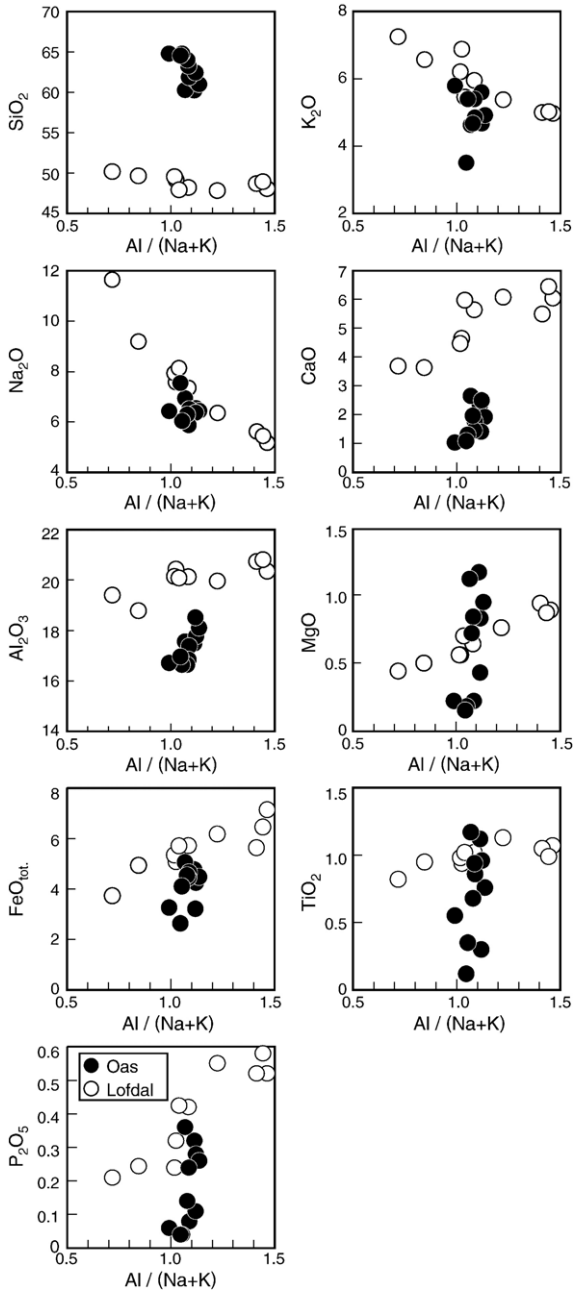

Fig. 4. Major element plots vs. molar Al/(Na+K) ratio for both types of syenite.

of 736+133/−141 Ma which is statistically similar to the 783±18 Ma concordia intercept age given by Burger and Kröner (unpublished data, cited in Tegtmeyer and Kröner, 1985) and the 764±60 Ma Rb–Sr whole rock age given by Hawkesworth et al. (1983). Additionally, Miller and Burger (1983) presented U–Pb zircon ages of 728±40 and 750±65 for alkali rhyolithes from the nearby Naauwpoort Formation which is probably genetically related to the syenites studied here. The most precise age constraint for the syenites is given by Hoffman et al. (1996) who presented a concordant U–Pb zircon age of 756±2 Ma for the Oas quartz-normative syenite. These results are confirmed by more recent U–Pb zircon ages of 752±7 Ma obtained on spatially associated quartz porphyries by De Kock et al. (2000). In order to resolve some the uncertainties regarding the age of both syenite occurrences, euhedral titanite of inferred primary magmatic origin was selected for geochronology and the results are reported in Table 1 and Fig. 3. Titanite was recovered from Oas and Lofdal samples and consists of euhedral yellow to brown grains. All selected fractions were free of visible inclusions. Most of the titanite fractions analyzed by conventional U–Pb techniques are nearly concordant and gave $^{207}Pb/^{206}Pb$ ages that range from 715±9 to

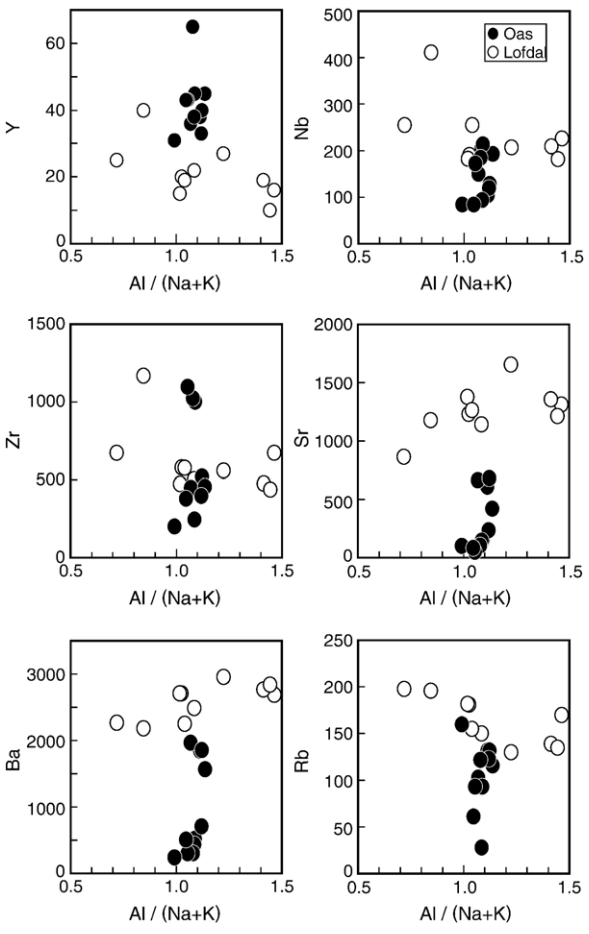

Fig. 5. Selected trace element plots vs. molar Al/(Na+K) ratio for both types of syenite.

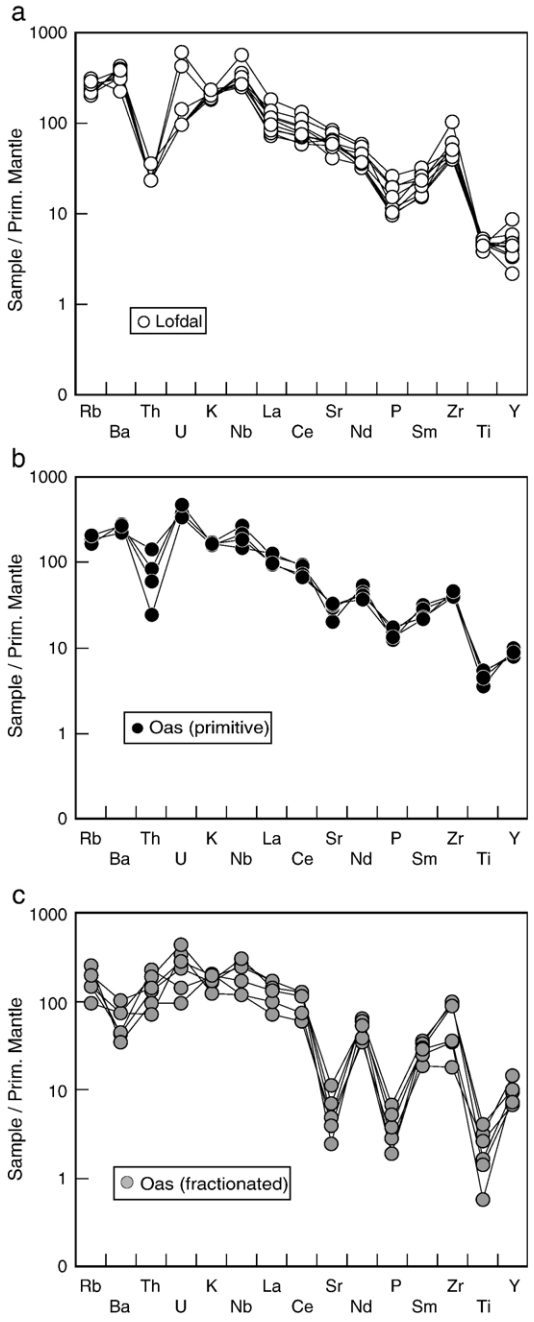

Fig. 6. Primitive-mantle normalized trace element diagram for both suites of syenites. Normalization factors from Sun and McDonough (1989).

751±4 Ma for the Lofdal syenites and from 737±5 to 758±7 Ma for the syenites from Oas (Table 1; Fig. 3). A weighted average of the $^{235}U/^{207}Pb$–$^{238}U/^{206}Pb$ ages for the Lofdal nepheline syenites gives an age of 754±8 Ma whereas a weighted average of the $^{235}U/^{207}Pb$–$^{238}U/^{206}Pb$ ages for the Oas quartz syenites yielded an age of 758±4 Ma. In view of the inferred magmatic origin of the euhedral titanites these ages are interpreted as the time of the emplacement of the syenites.

6. Geochemistry

6.1. Major and trace elements

Major and trace element compositions are given in Table 2 and Figs. 4 and 5. Due to the limited range in SiO_2 for most samples, the reverse alkalinity index (molar Al/(Na+K)) was used as an index of differentiation. For the nepheline-normative syenites from Lofdal, SiO_2 ranges from 47.8 to 50.2 wt.% and increases with decreasing molar Al/(Na+K) ratio. K_2O

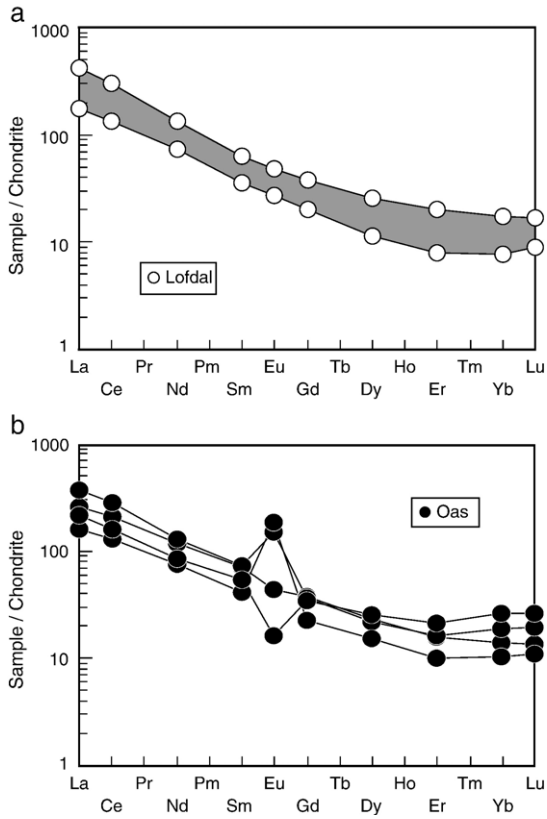

Fig. 7. Chondrite-normalized Rare Earth Element plots showing (a) the range of REE concentration for the Lofdal nepheline-normative syenites and (b) REE variations for selected samples of the quartz-normative Oas syenites. Normalization factors according to Boynton (1984). Note that the Lofdal nepheline-normative syenites are REE-enriched with no Eu anomaly whereas the Oas quartz-normative syenites have either a negative Eu anomaly due to fractionation of plagioclase and/or K-feldspar or develop a strong positive Eu anomaly due to accumulation of feldspar.

Table 3
Rb–Sr, Sm–Nd, Pb and O isotope data from Lofdal and Oas syenites (northern Damara orogen, Namibia)

		$^{87}Sr/^{86}Sr$ (m)	$^{87}Sr/^{86}Sr$ (i)	$^{87}Rb/^{86}Sr$	Rb (ppm)	Sr (ppm)	$^{143}Nd/^{144}Nd$ (m)	$^{143}Nd/^{144}Nd$ (i)	$^{147}Sm/^{144}Nd$	Sm (ppm)	Nd (ppm)	ε Nd (750 Ma)	T DM	$^{206}Pb/^{204}Pb$	$^{207}Pb/^{204}Pb$	$^{208}Pb/^{204}Pb$	$\delta^{18}O$
Lofdal	98/1.24	0.705771 (10)	0.703313	0.2296	134.1	1690	0.512215 (09)	0.511750	0.0945	12.17	77.88	1.55	1.07	18.036	15.608	37.818	8.2
Lofdal	98/1.23	0.706923 (12)	0.702972	0.3690	148.4	1163	0.512210 (10)	0.511749	0.0937	10.78	69.51	1.53	1.07	17.995	15.582	37.719	7.7
Lofdal	98/1.26	0.707242 (09)	0.703228	0.3749	166.9	1288	0.512220 (08)	0.511733	0.0991	8.946	54.58	1.21	1.11	18.002	15.602	37.776	7.4
Lofdal	98/1.25	0.706530 (11)	0.703449	0.2878	136.3	1370	0.512199 (06)	0.511721	0.0972	8.882	55.26	0.98	1.12	18.011	15.603	37.785	7.4
Lofdal	98/1.32	0.707407 (10)	0.702998	0.4118	176.0	1236	0.512198 (08)	0.511733	0.0946	8.351	53.37	1.21	1.10	18.022	15.601	37.787	7.0
Oas	KD 176	0.710176 (10)	0.703728	0.6022	127.4	612.1	0.512157 (07)	0.511647	0.0982	11.26	69.35	−0.07	1.19	n.d.	n.d.	n.d.	6.6
Oas	KD 177	0.708821 (10)	0.704015	0.4488	100.8	649.0	0.512155 (06)	0.511652	0.1013	10.84	64.70	−0.37	1.22	n.d.	n.d.	n.d.	6.9
Oas	KD 178	0.709782 (10)	0.703950	0.5447	128.8	683.9	0.512156 (12)	0.511695	0.0937	9.494	61.23	0.48	1.14	n.d.	n.d.	n.d.	6.4
Oas	98/1.33	0.711019 (10)	0.703197	0.7306	97.36	385.7	0.512252 (08)	0.511746	0.1029	13.96	82.02	1.47	1.10	18.006	15.593	37.758	6.5
Oas	98/1.37	0.725977 (10)	0.708306	1.6504	80.78	141.9	0.512171 (10)	0.511671	0.1016	11.64	69.26	0.01	1.19	18.200	15.604	37.864	6.9
Oas	98/1.36	0.722662 (09)	0.707719	1.3956	115.4	239.6	0.512166 (11)	0.511678	0.0993	11.45	69.67	0.14	1.18	18.120	15.601	37.821	7.1
Oas	98/1.34	0.710909 (09)	0.705989	0.4595	22.44	141.3	0.512169 (06)	0.511661	0.099	11.31	69.05	−0.18	1.39	18.069	15.592	37.762	6.5
Oas	KD 182	0.739585 (15)	0.705119	3.2190	115.5	104.1	0.512149 (06)	0.511645	0.1025	15.70	92.59	−0.50	1.23	n.d.	n.d.	n.d.	6.9
Oas	KD 184	0.763325 (12)	0.712172	4.7776	86.65	52.75	0.512089 (06)	0.511632	0.0929	14.62	95.15	−0.75	1.21	n.d.	n.d.	n.d.	7.1
Oas	KD 185	0.749935 (10)	0.704470	4.2463	148.0	101.2	0.512201 (09)	0.511680	0.1059	8.854	50.56	0.19	1.20	n.d.	n.d.	n.d.	6.9
Oas	98/1.35	0.731388 (09)	0.708688	2.1201	55.24	75.59	0.512187 (11)	0.511625	0.1142	9.793	51.85	−0.89	1.31	18.271	15.603	37.831	7.0

See Analytical techniques for analytical procedures. Uncertainties for the $^{87}Sr/^{86}Sr$ and $^{143}Nd/^{144}Nd$ are 2 σ (mean) errors in the last two digits. ε Nd values at the time of intrusion (Table 1) are calculated relative to CHUR with present day values of $^{143}Nd/^{144}Nd = 0.512638$ and $^{147}Sm/^{144}Nd$: 0.1966 (Jacobsen and Wasserburg, 1980). Nd model ages calculated with a depleted mantle reservoir and present-day values of $^{144}Nd/^{143}Nd$: 0.513144 and $^{147}Sm/^{144}Nd$: 0.222 (Michard et al., 1985). (m): measured, (i): initial., $\delta^{18}O$ values in per mil.

ranges from ca. 5.0 to ca. 6.9 wt.% and Na_2O ranges from ca. 5.2 to 11.7 wt.%. Both elemental abundances increase with decreasing molar Al/(Na+K) ratio. In contrast, abundances of MgO, $FeO_{(total)}$, TiO_2, CaO, P_2O_5 and Al_2O_3 decrease with decreasing molar Al/(Na+K) ratio. The quartz-normative syenites from Oas display only a limited range in molar Al/(Na+K) ratios. Therefore, most elemental abundances, i.e., K_2O (3.5–5.8 wt.%) and Na_2O (6.4–7.5 wt.%) show no clear correlation with the molar Al/(Na+K) ratio. There is however, a tendency for SiO_2 to increase and for CaO and Al_2O_3 to decrease with decreasing molar Al/(Na+K) ratio.

Nepheline-normative syenites from Lofdal are characterized by high concentrations of Ba (mostly >2000 ppm) and Sr (mostly >1000 ppm) whereas quartz-normative syenites from Oas have lower concentrations of Ba (<2000 ppm) and Sr (<1000 ppm). In both suites, Ba and Sr abundances decrease with decreasing molar Al/(Na+K) ratio (Fig. 5). Rb abundances are higher in samples from Lofdal and increase only in the samples from Lofdal with decreasing molar Al/(Na+K) ratio. High-Field-Strength-Elements (HFSE, Zr, Y, Nb) are high (Zr: 200–1170 ppm; Y: 10–65 ppm; Nb: <100–255 ppm) and increase with decreasing molar Al/(Na+K) ratio for the samples from Lofdal. Ni and Cr are very low (mostly <10 ppm) in all samples. Most Th and U abundances are higher in the quartz-normative syenites from Oas (Th: 2–19 ppm; U: 2–10 ppm) than in the nepheline-normative syenites from Lofdal where most samples have Th and U abundances close to the detection limit (2 ppm for Th and U).

Primitive mantle-normalized trace element patterns for Lofdal nepheline-normative syenites are similar to other trace element-enriched alkaline rocks (Foley et al., 1987; Gleason et al., 1994; Miller et al., 1999) with moderate depletions in Pb, Rb and Th relative to Ba and U (Fig. 6). They also show relative depletions in P and Ti but relative enrichments in Nb and Zr. Interestingly, the most mafic sample from Oas shows a similar trace element pattern than the nepheline-normative syenites from Lofdal. The differentiated samples from Oas have notably lower abundances for Ba, Sr, P and Ti but still have relative enrichments of Nb.

Rare Earth Element (REE) systematics are different for the samples from Lofdal and Oas (Fig. 7). For the nepheline-normative syenites from Lofdal, LREE concentrations are high with La abundances >400 times chondrite that decrease to <200 times chondrite. Yb concentrations are between 18 and 5 times chondrite and decrease with increasing differentiation. Chondrite-normalized La/Yb ratios range from ca. 20 to 50 with negligible Eu anomalies (Eu/Eu*: 0.9 to 1.1). For samples from Oas, La abundances range from ca. 400 times chondrite to 160 times chondrite whereas Yb concentrations are 10 to 19 times chondrite and generally increase with increasing differentiation. Chondrite-normalized La/Yb ratios range from ca. 9 to 25 in which some samples have no Eu anomaly and others develop strongly positive or negative Eu anomalies (Eu/Eu*: 0.4 to 6.4).

6.2. Strontium, Nd, Pb and O isotopes

The results of the Sr, Nd, Pb and O isotope analyses are reported in Table 3. Samples from the Lofdal nepheline-normative syenite complex have the most radiogenic Nd isotope composition so far recorded for Damaran igneous rocks with initial ε Nd (calculated for 750 Ma) ranging from +0.6 to +1.2. Syenites from the Oas complex have a larger range in initial ε Nd values ranging from +1 to −1.4. Initial $^{87}Sr/^{86}Sr$ ratios are also distinct and range from 0.70307 to 0.70352 for samples from Lofdal and from 0.70339 to 0.71367 for samples from Oas (Fig. 8). For samples from Lofdal initial ε Nd values tend to become less radiogenic with increasing SiO_2 whereas $^{87}Sr/^{86}Sr$ ratios are virtually unchanged. For samples from Oas, with increasing SiO_2 initial ε Nd values also become less radiogenic and $^{87}Sr/^{86}Sr$ ratios become more radiogenic (Fig. 9). Similarly, $^{206}Pb/^{204}Pb$ ratios are constant for syenites from Lofdal but increase

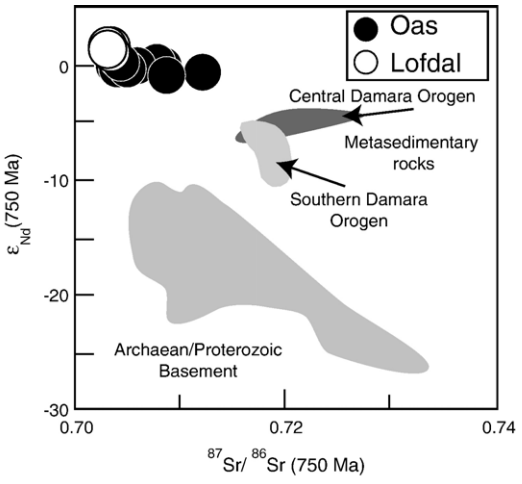

Fig. 8. Initial ε Nd vs. initial $^{87}Sr/^{86}Sr$ diagram for both types of syenite. Fields for metasedimentary rocks from the Damara orogen (with inferred depositional ages of >750 Ma) are from Jung (2005 and unpublished). Archaean to Proterozoic basement (recalculated to 750 Ma) is taken from Seth et al. (2002).

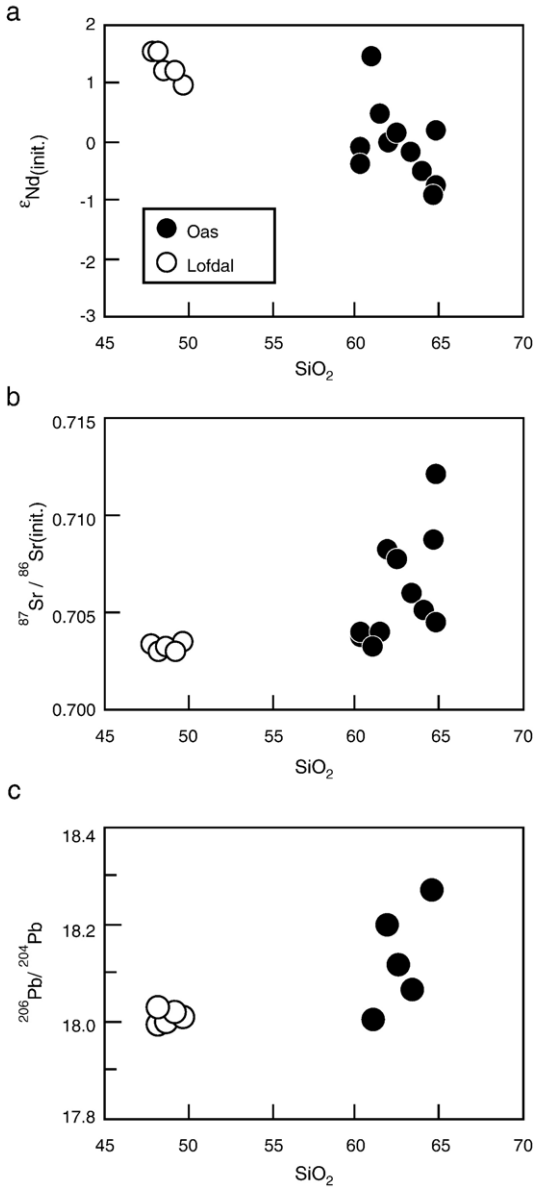

Fig. 9. Initial ε Nd, $^{87}Sr/^{86}Sr$ and $^{206}Pb/^{204}Pb$ vs. SiO_2 for both types of syenite. The trend for the Oas quartz-normative syenite is best explained by assimilation of felsic crustal rocks during fractional crystallization.

with increasing SiO_2 for syenites from Oas (Fig. 9). Generally, all syenite samples show rather high $\delta^{18}O$ values in which the variation of $\delta^{18}O$ for samples from Lofdal is between 7.0 and 8.2‰ and between 6.4 and 7.3‰ for samples from Oas. These values are mostly lower than those reported for other Damaran mafic rocks (7.8–9.9‰; Haack et al., 1982; Jung et al., 2002, 2004). In view of the highly alkaline nature and the radiogenic Nd but unradiogenic Sr isotope composition of the syenites, the lowest $\delta^{18}O$ values from the Lofdal and Oas samples are more typical of enriched mantle material than for mafic rocks that contain a crustal component. The $^{206}Pb/^{204}Pb$, $^{207}Pb/^{204}Pb$ and $^{208}Pb/^{204}Pb$ ratios obtained on acid-leached K-feldspar separated from both suites are almost identical to average upper crust with $\mu=9.74$ and $\kappa=4.0$ (Fig. 10; Stacey and Kramers, 1975). Lofdal nepheline-normative syenites show virtually no variation in $^{206}Pb/^{204}Pb$ and $^{207}Pb/^{204}Pb$ ratios but for the quartz-normative syenites from Oas there is some spread in $^{206}Pb/^{204}Pb$ ratios at more or less constant $^{207}Pb/^{204}Pb$ ratios. For the syenites from Lofdal, there is little variation of Pb isotopes with ε Nd values or $^{87}Sr/^{86}Sr$ ratios. On the other hand, for the Oas quartz-normative syenites, $^{206}Pb/^{204}Pb$ ratios increase with decreasing ε Nd values and increasing initial $^{87}Sr/^{86}Sr$ ratios (not shown in detail).

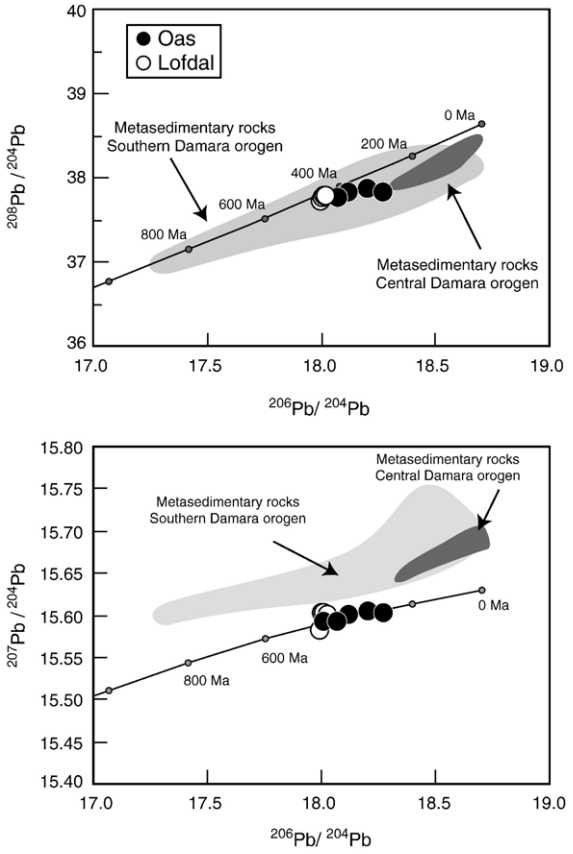

Fig. 10. Plot of (a) $^{207}Pb/^{204}Pb$ and (b) $^{208}Pb/^{204}Pb$ vs. $^{206}Pb/^{204}Pb$ isotope ratios of leached K-feldspar from both types of syenite. The curves represent average Pb growth curves according to Stacey and Kramers (1975) with $\mu=9.74$ and $\kappa=4.0$. Tick marks represent 200 Ma intervals. Fields for metasedimentary rocks from the Damara orogen (with inferred depositional ages of >750 Ma) are from Jung (2005 and unpublished).

7. Discussion

Simple models for the evolution of syenites that intrude into the continental crust do not exist. The generation and evolution of these rocks are controlled by the source mineralogy, the degree of melting, the fractional crystallization history and the likely crustal contamination. Additionally, due to the alkaline nature of such rocks, fluid-assisted alteration may have played a role. The isotope composition of many syenites is heterogeneous and this can be related to source heterogeneity, crustal contamination or alteration or a combination of these processes. Therefore, in order to place constraints on the composition of the mantle source it is necessary to evaluate first the effects of crystal fractionation and crustal contamination.

8. Fractional crystallization processes

Although the geochronological results indicate that both suites are coeval, samples with intermediate SiO_2 contents between 50 and 60 wt.% have not been observed and this feature may be related to the common occurrence of the Daly gap in alkaline rocks. Both suites of syenites are distinct and have a narrow range of SiO_2 contents, thus precluding a thorough quantification of crystal fractionation processes. However, samples from Lofdal show a considerable spread in the molar Al/(Na+K) ratio whereas this ratio is almost constant for the samples from Oas. For the nepheline-normative syenites from Lofdal, TiO_2, MgO, CaO, $FeO_{(total)}$, Al_2O_3 and P_2O_5 decrease with decreasing molar Al/(Na+K) ratio, indicating fractionation of early forming minerals i.e., clinopyroxene, amphibole, plagioclase or nepheline, Fe–Ti oxides and apatite. Nb and Zr abundances increase with decreasing molar Al/(Na+K) ratio indicating that titanite and zircon which are important hosts for these elements were not important during fractional crystallization processes. Trace elements with a high distribution coefficient for feldspar minerals (Ba and Sr) decrease with decreasing molar Al/(Na+K) ratio. Samples from Oas have only a narrow range in molar Al/(Na+K) ratios, however, SiO_2 tend to increase and CaO, Al_2O_3, Ba and Sr tend to decrease with decreasing molar Al/(Na+K) ratio. Based on these semiquantitative observations, it can be concluded that the syenites from Lofdal and Oas cannot be linked by the same differentiation process because these elements do not follow the same inferred liquid line of descend.

From the Ba–Sr diagram (Fig. 11) it is seems obvious that the variation in Ba and Sr abundances in both suites must be explained by fractionation/accumulation of

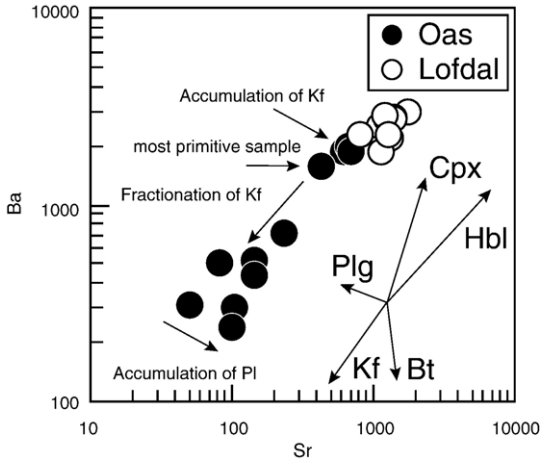

Fig. 11. Variation of Ba vs. Sr concentration within the syenites. Mineral vectors calculated according to partition coefficients compiled in Rollinson (1993). Compositional trend of the syenites indicates complex processes of fractionation or accumulation of K-feldspar for most samples, however, some samples are additionally influenced by accumulation of plagioclase.

mainly feldspar. Accumulation of amphibole may also have played a role in generating this positive correlation although there is no conclusive petrographic evidence for this because only a few samples are characterized by glomerophyric clots of amphibole. For the samples from Lofdal, the decrease in Ba and Sr and increase in Rb with decreasing molar Al/(Na+K) ratios suggest that fractionation of K-feldspar played a significant role here. On the other hand, the observation that the bulk rock chemical composition of the samples from Oas with SiO_2: 60–65 wt.%, Na_2O: 6–8 wt.% and K_2O: 4–6 wt.% is broadly similar to a 50:50 mixture of Na-feldspar and K-feldspar suggests that these samples are more likely products of a complex fractionation/unmixing process involving mainly feldspar. Moreover, the similar molar Al/(Na+K) ratios of Na-feldspar and K-feldspar (1.06 and 1.07, respectively; Deer et al., 1992) and the Oas quartz-normative syenites (0.99–1.04) seem to support this hypothesis. The most primitive sample from Oas (sample 98/1.33) has a Ba content of 1567 ppm, a Sr content of 422 ppm and a negligible negative Eu anomaly (Eu/Eu*: 0.97). This sample is considered to represent the most primitive sample (Fig. 11). Three samples have higher Sr and abundances and slightly positive Eu anomalies ranging from 1.26 to 1.36 indicating limited amounts of K-feldspar accumulation. Four other samples are characterized by lower Sr and Ba abundances than sample 98/1.33 and together with their slightly positive to strongly negative Eu anomalies (Eu/Eu*: 1.08 to 0.39) implies that these samples had undergone fractionation of

mainly K-feldspar. The remaining three samples have the lowest Ba abundances but increased Sr abundances and the most prominent positive Eu anomalies with Eu/Eu* ratios ranging from 3.2 to 6.5. These features suggest that accumulation of plagioclase had affected these samples.

In conclusion, the major and trace element variations displayed by the nepheline-normative syenites from Lofdal suggest that crystal–liquid fractionation played an important role in the petrogenesis of these syenites. In such a simple model, the variations of MgO, $FeO_{(total)}$, CaO and TiO_2 with molar Al/(Na+K) ratio as an index of differentiation are due to crystallization and removal of early crystallized mafic minerals such as clinopyroxene, amphibole and titanomagnetite. However, for the quartz-normative syenites from Oas, a more complex model of fractional crystallization-cumulate and melt unmixing (e.g., Cullers et al., 1993) seems to be more likely. The ubiquitous presence of large K-feldspar phenocrysts in some samples suggests that separation of these early crystallized cumulate crystals was incomplete. In a cumulate–melt unmixing model, varying concentrations of Ba and Sr, slightly negative, moderate positive or strongly positive Eu anomalies together with SiO_2 abundances and molar Al/(Na+K) ratios of the syenites similar to average Na-feldspar and K-feldspar may point to complex K-feldspar/plagioclase accumulation/fractionation during the evolution of these syenites.

9. Assimilation processes

Based on the regular variation of major and trace element abundances fractional crystallization of mainly clinopyroxene, amphibole, plagioclase or nepheline, Fe–Ti oxides and apatite together with limited accumulation of K-feldspar and plagioclase is considered as the predominant process for the evolution of the syenites from Oas and Lofdal. However, it is likely that the majority of continental syenites were generated by interaction between mantle-derived alkali basaltic melts and pre-existing continental crust. Fitton (1987) and Foland et al. (1993) proposed that assimilation of continental crust is essential for a nepheline-normative magma to evolve across the thermal divide in the quartz–nepheline–kalsilite system in order to produce a quartz-normative syenitic melt. The thermal divide is known to persist until at least 10 kbar although this has been tested experimentally only for $P_{H2O}=P_{total}$ (Morse, 1970), a situation that is rarely achieved in natural magmas except at the very latest stage of crystallization. Application to natural magmas requires a knowledge of the equilibria under conditions of $P_{H2O}<P_{total}$ and $P_{total}=P_{H2O+CO2}$ and it is therefore possible that at higher pressures and distinct fluid compositions polybaric fractionation may account for the coeval occurrence of silica-undersaturated and silica-saturated syenites.

Neodymium, Sr, Pb and O isotope data reveal a noticeable role of crustal contamination in the generation of the more evolved quartz-normative syenite magmas from Oas, most probably via a concurrent crustal assimilation and fractional crystallization process (AFC; DePaolo, 1981). However, calculation of AFC curves are strongly model dependent, because they require assumptions about the fractionating mineral assemblage and mineral-melt distribution coefficients, the concentrations of the respective trace elements in the starting melt and the contaminant and the ratio of assimilation to fractional crystallization (*r*-value).

The Lofdal nepheline-normative syenites show no significant variation in Sr and Pb and only a minor variation in Nd isotope composition and therefore crustal contamination may have played no significant role in the evolution of these rocks. On the other hand, for the quartz-normative syenites from Oas, initial $^{87}Sr/^{86}Sr$ and $^{206}Pb/^{204}Pb$ ratios increase whereas initial ε Nd values decrease with increasing SiO_2 (Fig. 9). Similarly, $\delta^{18}O$ values increase with increasing initial $^{87}Sr/^{86}Sr$ ratios and decreasing initial ε Nd values (Fig. 12). These features are qualitatively consistent with assimilation of crustal material that can be expected to have higher $^{87}Sr/^{86}Sr$ and $^{206}Pb/^{204}Pb$ ratios, higher $\delta^{18}O$ and lower ε Nd values. Based on field evidence it is very likely that contamination involved basement-derived gneisses of the Huab gneiss domain which occurred either in the deeper crust or close to the present level of exposure.

Fig. 13 reports the result of two model calculations, one involving metasedimentary rocks and the other basement-derived material as the contaminant. Unfortunately, no isotope data are available from the basement gneisses or from metasedimentary rocks from this particular part of the Damara orogen. However, some semiquantitative constraints can be placed by using published isotope data from pre-Pan-African gneisses from the nearby Kaoko Belt (Seth et al., 2002), situated farther north from the Huab gneiss domain and also from isotope data from Damaran metasedimentary rocks (McDermott et al., 1989; McDermott and Hawkesworth, 1990; Jung, 2005; unpublished). The pre-Pan-African gneisses from the Kaoko belt range in age from 2.5 Ga to 1.5 Ga (Seth et al., 1998) and the Huab gneiss has an age of ca. 1.8 Ga (Tegtmeyer and Kröner, 1985). There

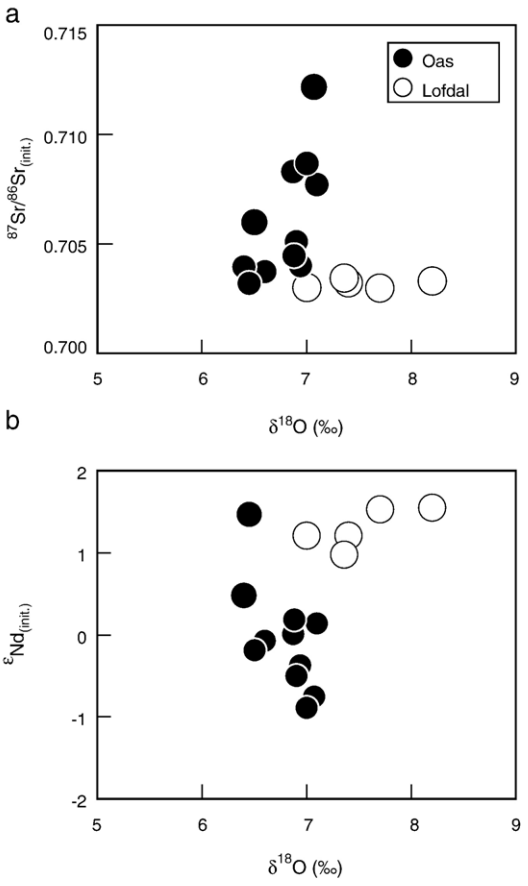

Fig. 12. Plot of (a) $\delta^{18}O$ vs. $^{87}Sr/^{86}Sr$ and (b) $\delta^{18}O$ vs. ε Nd.

is, however, good evidence that parts of the Huab gneiss domain consist of older material up to 2.12 Ga (Tegtmeyer and Kröner, 1985). Assuming that the Huab gneisses have similar isotope compositions than the pre-Pan-African basement rocks from the Kaoko belt (Seth et al., 2002), their slightly more radiogenic $^{87}Sr/^{86}Sr$ ratios (recalculated at 750 Ma) but significantly more unradiogenic ε Nd values of <-10 (at 750 Ma) make some of these rocks likely endmembers in AFC calculations. Similarly, most basement samples have $\delta^{18}O$ values between 7 and 10‰ (Seth et al., 2002) further suggesting that such rocks may serve as suitable contaminants.

The 750 Ma age of the syenites is similar to the ages of the spatially associated Naauwpoort alkali rhyolites which intruded the metasedimentary rocks of the Nosib Group (Miller and Burger, 1983). Depositional ages of Nosib metasedimentary rocks are believed to be around 850 Ma whereas other metasedimentary rocks from the belt have younger depositional ages of ca. 600 Ma (McDermott et al., 1989). However, only a few of the Etusis and Khan Formation metasedimentary rocks (which are members of the Nosib group) have $^{87}Sr/^{86}Sr$ ratios low enough and ε Nd values (at 750 Ma) between −3 and −6 to serve as probable contaminants. Other hypothetical contaminants may include igneous rocks with emplacement ages close to those of the syenites

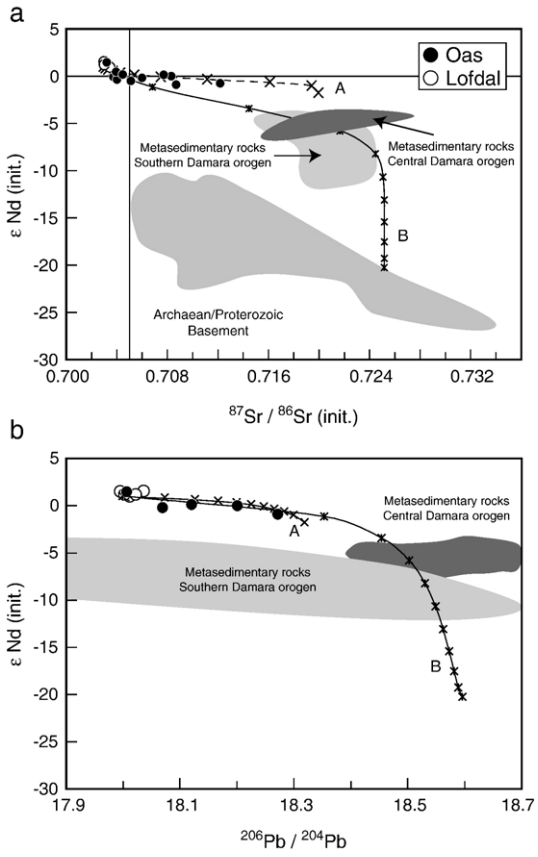

Fig. 13. AFC calculations for the Oas quartz-normative syenite using initial ε Nd vs. (a) $^{87}Sr/^{86}Sr$ and (b) $^{206}Pb/^{204}Pb$ isotope compositions. Assimilation of upper crustal sedimentary rocks (A) is best modeled with a hypothetical parental syenite melt with 100 ppm Nd ($^{143}Nd/^{144}Nd$: 0.511720, $\varepsilon Nd_{(750\ Ma)}$: +1), 1500 ppm Sr ($^{87}Sr/^{86}Sr_{(750\ Ma)}$: 0.703) and 6 ppm Pb ($^{206}Pb/^{204}Pb$: 18.00). The contaminant has 30 ppm Nd ($^{143}Nd/^{144}Nd$: 0.511400, $\varepsilon Nd_{(750\ Ma)}$: −5.3), 100 ppm Sr ($^{87}Sr/^{86}Sr_{(750\ Ma)}$: 0.720), 20 ppm Pb, $^{206}Pb/^{204}Pb$: 18.30). The *r*-value (ratio of assimilation to fractional crystallization) was fixed at 0.4. Kd's for Sr, Nd and Pb were 2.5, 0.5 and 0.3. Tick marks represent 10% intervals. Assimilation of lower crustal basement rocks (B) is best modeled with a hypothetical parental syenite melt with 100 ppm Nd ($^{143}Nd/^{144}Nd$: 0.511720, $\varepsilon Nd_{(750\ Ma)}$: +1), 1500 ppm Sr ($^{87}Sr/^{86}Sr_{(750Ma)}$: 0.703) and 6 ppm Pb ($^{206}Pb/^{204}Pb$: 18.00). The contaminant has 25 ppm Nd ($^{143}Nd/^{144}Nd$: 0.510630, $\varepsilon Nd_{(750\ Ma)}$: −20), 386 ppm Sr ($^{87}Sr/^{86}Sr_{(750\ Ma)}$: 0.725205), 20 ppm Pb, $^{206}Pb/^{204}Pb$: 18.60). Nd and Sr isotope compositions and elemental abundances are taken from Seth et al. (2002; their sample BK 446 a). The *r*-value (ratio of assimilation to fractional crystallization) was fixed at 0.8. Kd's for Sr, Nd and Pb were 2.5, 0.5 and 0.3. Tick marks represent 10% intervals.

(i.e., between 1.0 and 0.8 Ga) and evolved isotope characteristics (ε Nd: −1 to −4, $^{87}Sr/^{86}Sr$: 0.715–0.720, $\delta^{18}O$: ca. 7‰, i.e., Allègre and Ben Othman, 1980). However, such rocks have not been described from the Damara orogen.

Due to high concentrations of Sr and Nd but low concentrations of Pb in the inferred parental syenites, modelling of contamination processes is strongly depended on the ratio of assimilation to fractional crystallization (*r*-value). In the model of lower crustal assimilation that used basement-derived rocks as the contaminant, the rate of assimilation to fractional crystallization was set to 0.8. Such a high ratio is not unlikely considering the high temperature of the inferred parental alkali basaltic melt and the moderate to high ambient temperatures of lower crustal rocks (i.e., Reiners et al., 1995). Note that even the samples that do not represent true liquids, i.e., those that have large positive Eu anomalies indicative of accumulation of feldspar possess evolved isotope compositions. This feature suggests that assimilation must have occurred before accumulation, implying a deep crustal site for AFC processes. The resulting amount of assimilation is <15% (Fig. 13a). In $^{206}Pb/^{204}Pb$ vs. ε Nd, assimilation can be modeled using a Pb isotope composition for the upper mantle source of $^{206}Pb/^{204}Pb = 18.0$ corresponding to the most primitive syenite and for the lower crustal component of $^{206}Pb/^{204}Pb = 18.6$, compatible with Pb isotope composition from the basement of the Damara orogen (Jung et al., 2003). Estimated amounts of assimilation are <10% (Fig. 13b). The view of lower crustal assimilation is also supported by the presence of inherited 2.12 Ga-old zircon in the Oas syenite (Tegtmeyer and Kröner, 1985).

For the case of upper crustal assimilation, combined AFC model calculations used a crustal component with $^{87}Sr/^{86}Sr_{(750\ Ma)}$: 0.725, $\varepsilon\ Nd_{(750\ Ma)}$: −5, and $^{206}Pb/^{204}Pb_{(750\ Ma)}$: 18.30. These isotope compositions are reasonable average values for Etusis metasedimentary rocks (McDermott and Hawkesworth, 1990). The rate of assimilation to fractional crystallization was set to 0.4. In this scenario, a lower *r*-value must be used because of the inferred low temperature of evolved syenite melts that were emplaced in relatively cold upper crustal levels. The major difference to the model of lower crustal assimilation is that the amount of assimilation is extremely high with values between 60 and 70%. In view of the alkaline nature of the syenites, this model is therefore considered to be unlikely. In conclusion, the Lofdal nepheline-normative syenites and the primitive members from the Oas quartz-normative syenites seem to represent uncontaminated upper mantle derived alkaline melts. More evolved quartz-normative syenites were subsequently modified by contamination with a lower crustal component.

10. The mantle source of the parent magma(s) for the syenites

The nepheline-normative nature of the Lofdal syenites indicates that these melts were generated by partial melting of upper mantle material because it is impossible that nepheline-normative melts can be generated by partial melting of common crustal rocks which are strongly quartz-normative (Taylor and McLennan, 1985; Foland et al., 1993). Moreover, the high total alkali contents observed here (Na_2O+K_2O: 11–17 wt.%) are different to those observed in upper or lower crustal rocks which have significantly lower Na_2O+K_2O contents of 7.3 wt.% and 3.1 wt.%, respectively (Taylor and McLennan, 1985). The major element characteristics of the syenites with molar Al/(Na+K) ratios between 0.8 and 1.3 are further distinct to those observed in upper crustal (molar Al/(Na+K): 1.5) or lower crustal rocks (molar Al/(Na+K): 3.2). Most samples have low La/Nb, Ba/Nb (Fig. 14) and Zr/Nb ratios. The primitive samples from Lofdal have high Ce/Pb ratios that are correlated with low Pb concentrations, low $^{206}Pb/^{204}Pb$ ratios and low initial $^{87}Sr/^{86}Sr$ ratios (Fig. 15). These features also indicate involvement of upper mantle sources in which the absence of negative Nb anomalies in primitive mantle-normalized diagrams (Fig. 6) indicate no role for a subduction-related crustal

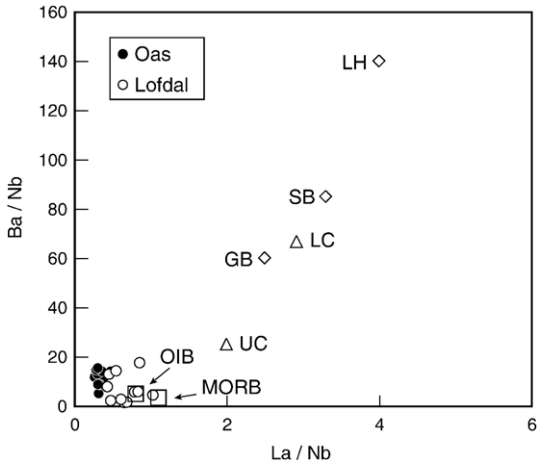

Fig. 14. La/Nb vs. Ba/Nb for Oas and Lofdal syenites. MORB and OIB estimates are from Sun and McDonough (1989), upper crust (UC) and lower crust (LC) are from Taylor and McLennan (1985) and some alkaline rocks (LH, Leucite Hills; SB, Smoky Butte; GB, Gaussberg) are form Mitchell and Bergman (1991).

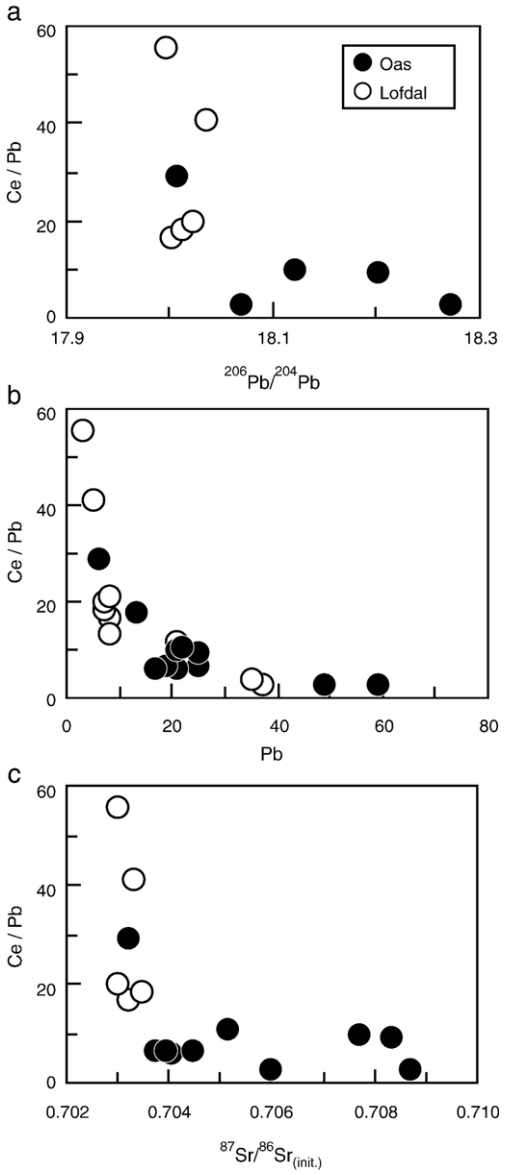

Fig. 15. Plot of (a) Ce/Pb vs. Pb, (b) Ce/Pb vs. initial $^{87}Sr/^{86}Sr$ and (c) Ce/Pb vs. $^{206}Pb/^{204}Pb$.

component in the source of the primitive syenites. Moreover, the most primitive syenites from Lofdal and Oas have high Ti/Y (200–400), high Ce/Pb (>16), high Sr/Nd (10–30) and low Ce/Sr (0.10–0.18), low Rb/Ba (<0.08) and low Rb/Sr (<0.16) ratios. The isotope composition of the Lofdal nepheline-normative syenites and the primitive members of the Oas quartz-normative syenites indicate that they were derived from a source depleted in Rb and LREE relative to Bulk Earth. The inferred upper mantle source has probably an ε Nd value of ca. +1 and $^{87}Sr/^{86}Sr$ close to 0.703 which are reasonable values for moderately depleted upper mantle components. The oxygen isotope value of the most primitive sample from the nepheline-normative syenites from Lofdal is ca. 7‰. There is, however, a tendency for the oxygen isotope values to increase with increasing Fe^{3+}/Fe^{2+} and increasing sum of volatiles (expressed as loss on ignition, LOI) indication that oxidizing and hydrous alteration affected the isotope composition (Fig. 16). Extrapolating back to a hypothetical syenite with Fe^{3+}/Fe^{2+} of 0.5 and an LOI value of 1 wt.% indicates a near-primary $\delta^{18}O$ value of 6.5‰. This inferred near-primary $\delta^{18}O$ value of 6.5‰ is similar to the average $\delta^{18}O$ value of 6.2±0.7‰ (Harmon and Hoefs, 1993) of continental mantle-derived alkaline basalts. The quartz-normative syenites from Oas have similar $\delta^{18}O$ values which are not correlated with LOI values or Fe^{3+}/Fe^{2+} ratios. This feature indicates that in this case hydrous alteration did not change the oxygen isotope composition although some samples show similar high Fe^{3+}/Fe^{2+} ratios. For the samples from Oas, ε Nd values are negatively and Sr isotope ratios are positively correlated with $\delta^{18}O$ values (Fig. 12) suggesting that crustal contamination is responsible for the increase in $\delta^{18}O$ from 6.5‰ to 7‰.

Similarly, Pb isotopes are very sensitive indicators of source characteristics. The values obtained on leached K-feldspar from the least contaminated samples which

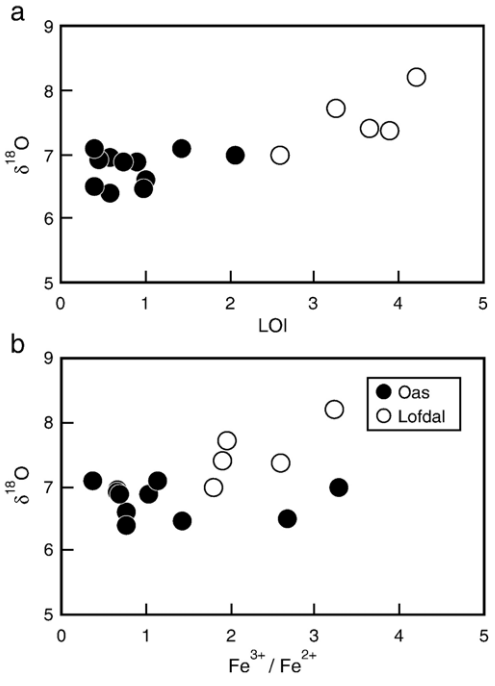

Fig. 16. Plot of (a) $\delta^{18}O$ vs. Fe^{3+}/Fe^{2+} and (b) $\delta^{18}O$ vs. LOI. LOI is loss on ignition.

are interpreted to represent initial values based on the high Pb but negligible U content in feldspar, are higher than likely values for the depleted upper mantle at that time and plot on the $^{207}Pb/^{204}Pb$–$^{206}Pb/^{204}Pb$ evolution curve with μ=9.74 (Fig. 10; Stacey and Kramers, 1975). In view of the alkaline nature of the syenites this slightly enriched Pb isotope composition is interpreted to reflect an upper mantle source with higher U/Pb ratios relative to the depleted upper mantle. Furthermore, the $^{207}Pb/^{204}Pb$ ratios are lower than measured ratios for sedimentary rocks from the central and southern Damara orogen (McDermott and Hawkesworth, 1990; Jung, 2005; unpublished). Because the metasedimentary rocks studied by McDermott and Hawkesworth (1990) underwent post-depositional U mobility it is not possible to calculate initial depositional isotope ratios for these samples. However, it seems evident that the Pb isotope characteristics exclude such Damaran metasedimentary crust as a potential source for the variation in Pb isotope composition. Much of the variation in $^{206}Pb/^{204}Pb$ of the quartz-normative syenites from Oas can be attributed to contamination with a crustal component (Fig. 9c). However, the most primitive and by implication uncontaminated samples from Oas show similar Pb isotope characteristics than the nepheline-normative syenites from Lofdal. It is therefore concluded that the parental magmas of both syenite suites originated from a pre-Pan-African lithospheric mantle source with time-integrated slightly elevated U/Pb and Th/U ratios. One possible model is to ascribe the Pb isotope compositions to a metasomatized upper mantle lithospheric component that was isolated for a considerable period of time from the convecting part of the upper mantle before the partial melting event.

Thompson and Fowler (1986) have shown, that for known or generally accepted geotectonic settings, Zr–Nb variations in alkaline rocks differ between those from subduction-related and post-collisional settings and those which are associated with continental extension away in space and time from subduction. The syenites analyzed here have high Zr (400–1100 ppm) and high Nb (>200 ppm) concentrations and have positively correlated Zr and Nb concentrations that support the almost similar geochemical behaviour of these elements and hence their similar bulk Kd's. The high concentrations of these elements are typical for alkaline rocks remote from subduction zones in space and time and are more characteristic for extension-related tectonic settings (Thompson and Fowler, 1986). Moreover, ocean island basalts (OIB) and continental alkaline basalts (CAB) and their products of differentiation commonly have La/Nb ratios <1 whereas alkaline magmas emplaced in subduction zone settings have higher La/Nb ratios (La/Nb: 3–12, Thompson and Fowler, 1986; Thirlwall and Burnard, 1990; Fowler, 1992). Therefore, the low La/Nb ratios between 0.3 and 0.9 for uncontaminated members of the Oas and Lofdal syenites (Fig. 14) are again indicative for alkaline melts emplaced in an extension-related environment.

11. Summary and conclusion

For the Neo-Proterozoic nepheline-normative syenites from Lofdal and for the uncontaminated quartz-normative syenites from Oas, there is good evidence for the involvement of a moderately depleted subcontinental upper mantle component indicated by depleted isotopic compositions, low La/Nb, Rb/Ba, Rb/Sr and Sr/Ce ratios but high Ce/Pb, Sr/Nd and Ti/Y ratios. Only for the nepheline-normative syenites from Lofdal, a simple, two-stage model involving partial melting of upper mantle material followed by differentiation of an unexposed alkali basaltic magma can account for the geochemical and isotopic composition. For the quartz-normative syenites from Oas, the following more complex processes were involved: (i) partial melting of a moderately depleted upper mantle to produce an inferred nepheline-normative parental melt, (ii) assimilation of lower crustal rocks to produce the quartz-normative syenites with evolved isotope characteristics, (iii) emplacement of discrete magma batches into the local continental crust and subsequent (iv) crystal fractionation/cumulate-melt unmixing processes to produce the individual samples. Therefore, a generalized model for the origin of contemporaneous nepheline-normative and quartz-normative syenites apparently fails to explain how such melts could effectively segregate from a mantle source and be emplaced into high crustal levels. One important factor is the intimate association of the syenites with the northern rift flank of the Neo-Proterozoic intracontinental rift which later gave rise to the intracontinental branch of the Damara orogen. After final assembly of the Proterozoic basement complexes upwelling of hot asthenospheric mantle material caused intracontinental rifting, pressure release, channeling of volatiles, partial melting and generation of alkaline magmas from the subcontinental upper mantle. Subsequently, some of these alkaline magmas evolved via an AFC process in crustal magma chambers. In a plate-tectonic context, a correlation between alkaline magmatism and intracontinental rifting indicates the activation of lithospheric zones of weakness during rifting which may have promoted fast ascent and intrusion of the parental melts. In this

model, access to previously unsampled mantle sources is due to the rise of mantle material to shallow depths beneath continental lithosphere after rupture of the cold lithospheric plate. While the source of the alkaline rocks is in the lithospheric mantle, their location is controlled by the structure, composition and dynamics of the overlying continental crust. Rift-related magmatism at about 750 Ma is widespread in southern Gondwana and is presumably associated with fragmentation of a Neo-Proterozoic supercontinent. Such magmatism occurred also in northwestern India (Kochar, 1990) in which this area also evolved into a continental margin bordering the Mozambique craton.

Acknowledgements

The radiogenic isotope analyses were supported by the Max-Planck-Society and A.W. Hofmann is thanked for hospitality and free access to mass spectrometry facilities while S. J. held a post-doc position in Mainz. Iris Bambach (Max-Planck-Institut, Mainz) did a superb job in managing the line drawings. Special thanks go to D. Dohle from the Bonn fluorine-lab crew for the determination of the oxygen isotope ratios. S. Göbeler (Marburg) helped with Fe^{2+} and REE determinations. A. Kröner (Mainz) is thanked for providing samples labelled KD. We also appreciate the help of Bob Trumbull, Peter Dulski and Christa Wiesenberg (all GFZ Potsdam) in providing REE analyses for some samples at short notice. Two anonymous journal reviewers made numerous comments that were helpful in revising the manuscript.

References

Allègre, C.J., Ben Othman, D., 1980. Nd–Sr relationship in granitoid rocks and continental crust development: a chemical approach to orogenesis. Nature 286, 335–342.

Asprey, L.B., 1976. The preparation of very pure fluorine gas. Fluor. Chem. 7, 359–361.

Blichert-Toft, J., Arndt, N.T., Ludden, J.N., 1996. Precambrian alkaline magmatism. Lithos 37, 97–111.

Boynton, W.V., 1984. Geochemistry of rare earth elements: meteorite studies. In: Henderson, P. (Ed.), Rare Earth Element Geochemistry. Elsevier, New York, pp. 63–114.

Brotzu, P., Gomes, C.B., Melluso, L., Morbidelli, L., Morra, V., Ruberti, E., 1997. Petrogenesis of coexisting SiO_2-undersaturated to SiO_2-oversaturated felsic igneous rocks: the alkaline complex of Itatiaia, Southeastern Brazil. Lithos 40, 133–156.

Brown, P.E., Becker, S.M., 1986. Fractionation, hybridisation, and magma mixing in the Kialineq centre, East Greenland. Contrib. Mineral. Petrol. 92, 57–70.

Bühn, B., Okrusch, M., Woermann, E., Lehnert, K., Hoernes, S., 1995. Metamorphic evolution of Neoproterozoic manganese formations and their country rocks at Otjosondu, Namibia. J. Petrol. 36, 463–496.

Cameron, A.E., Smith, D.H., Walker, R.L., 1969. Mass spectrometry of nanogram-size samples of lead. Anal. Chem. 41, 525–526.

Clayton, R.N., Mayeda, T.D., 1963. The use of bromine pentaflouride in the extraction of oxygen from oxides and silicates for isotope analysis. Geochim. Cosmochim. Acta 27, 43–52.

Cullers, R.L., Stone, J., Anderson, L., Sassarini, N., Bickford, M.E., 1993. Petrogenesis of Mesoproterozoic Oak Creek and West McCoy Gulch plutons, Colorado: an example of cumulate unmixing of a mid-crustal, two-mica granite of anorogenic affinity. Precambrian Res. 62, 139–169.

Dawson, J.B., 1987. The kimberlite clan: relationship with olivine and leucitite lamproites, and inferences for upper mantle metasomatism. In: Fitton, J.G., Upton, B.G. (Eds.), Alkaline Igneous Rocks. Geol. Soc. Spec. Publ., vol. 30, pp. 95–101.

Deer, W.A., Howie, R.A., Zussman, J., 1992. An introduction to the rock-forming minerals. Longman Scientific and Technical. Wiley and Sons, New York. 696 pp.

De Kock, G.S., Eglington, B., Armstrong, R.A., Harmer, R.E., Walraven, F., 2000. U–Pb and Pb–Pb ages of the Naauwpoort rhyolite, Kawakeup leptite and Okongava diorite: implications for the onset of rifting and orogenesis in the Damara belt, Namibia. Commun. Geol. Surv. Namib. 12, 81–88.

DePaolo, D.J., 1981. Trace element and isotopic effects of combined wallrock assimilation and fractional crystallization. Earth Planet. Sci. Lett. 53, 189–202.

Downes, H., 1987. Tertiary and Quarternary volcanism in the Massif Central, France. In: Fitton, J.G., Upton, B.G. (Eds.), Alkaline Igneous Rocks. Geol. Soc. Spec. Publ., vol. 30, pp. 517–530.

Dulski, P., 2001. Reference materials for geochemical studies: new analytical data by ICP-MS and critical discussion of reference values. Geostand. Newsl. 25, 87–125.

Ewart, A., 1982. Petrogenesis of the Tertiary anorogenic volcanic series of Southern Queensland, Australia, in the light of trace element geochemistry and O, Sr, and Pb isotopes. J. Petrol. 23, 344–382.

Fitton, J.G., 1987. The Cameroon line, West Africa: a comparison between oceanic and continental alkaline volcanism. In: Fitton, J.G., Upton, B.G. (Eds.), Alkaline igneous rocks. Geol. Soc. Spec. Publ., vol. 30, pp. 273–291.

Fitton, J.G., Upton, B.G., 1987. Alkaline igneous rocks. Geol. Soc. Spec. Publ. 30 568 pp.

Foland, K.A., Landoll, J.D., Henderson, C.M.B., Jiangfeng, C., 1993. Formation of cogenetic quartz and nepheline syenites. Geochim. Cosmochim. Acta 57, 697–704.

Foley, S.F., Venturelli, G., Green, D.H., Toscani, L., 1987. The ultrapotassic rocks: characteristics, classification, and constraints for petrogenetic models. Earth Sci. Rev. 24, 81–134.

Fowler, M.B., 1992. Elemental and O–Sr–Nd isotope geochemistry of the Glen Dessary syenite, NW Scotland. J. Geol. Soc. (Lond.) 149, 209–220.

Gleason, J.D., Miller, C.V., Wooden, J.L., Bennett, V.C., 1994. Petrogenesis of the highly potassic 1.42 Ga Barrel Spring pluton, southeastern California, with implications for mid-Proterozoic magma genesis in the southwestern USA. Contrib. Mineral. Petrol. 118, 182–197.

Haack, U., Hoefs, J., Gohn, E., 1982. Constraints on the origin of Damaran granites by Rb/Sr and $\delta^{18}O$ data. Contrib. Mineral. Petrol. 79, 279–289.

Harmon, R.S., Hoefs, J., 1993. Oxygen Isotopes in Neogene Volcanic Rocks—A Global Data Base. Report AvH Foundation. Geochemisches Institut der Georg August Universität Göttingen, Germany.

Harris, N.B.W., Duyverman, H.J., Almond, D.C., 1983. The trace element and isotope geochemistry of the Sabaloka Igneous Complex, Sudan. J. Geol. Soc. (Lond.) 140, 245–256.

Hartmann, O., Hoffer, E., Haack, U., 1983. Regional metamorphism in the Damara orogen: interaction of crustal motion and heat transfer. Spec. Publ. - Geol. Soc. S. Afr. 11, 233–241.

Hawkesworth, C.J., Gledhill, A.R., Roddick, J.C., Miller, R.Mc.G., Kröner, A., 1983. Rb–Sr and $^{40}Ar/^{39}Ar$ studies bearing on models for the thermal evolution of the Damara belt. Spec. Publ. - Geol. Soc. S. Afr. 11, 323–338.

Heinrichs, H., Herrmann, A.G., 1990. Praktikum der Analytischen Geochemie. Springer Verlag, Berlin.

Hoffman, P.F., Hawkins, D.P., Isachsen, C.E., Bowring, S.A., 1996. Precise U–Pb zircon ages for early Damaran magmatism in the Summas Mountains and Welwitschia inlier, northern Damara belt, Namibia. Commun. Geol. Surv. Namib. 11, 47–52.

Jacobsen, S.B., Wasserburg, G.J., 1980. Sm–Nd isotopic evolution of chondrites. Earth Planet. Sci. Lett. 50, 139–155.

Jung, S., 2005. Isotopic equilibrium/disequilibrium in granites, metasedimentary rocks and migmatites (Damara orogen, Namibia)—a consequence of polymetamorphism and melting. Lithos 84, 168–184.

Jung, S., Mezger, K., 2001. Geochronology in migmatites—A Sm–Nd, U–Pb and Rb–Sr study from the Proterozoic Damara belt (Namibia) and implications for polyphase development of migmatites in high-grade terranes. J. Metamorph. Geol. 19, 77–97.

Jung, S., Mezger, K., 2003. Petrology of basement-dominated terranes: I. Regional metamorphic T-t path from U–Pb monazite and Sm–Nd garnet chronology (Central Damara orogen, Namibia). Chem. Geol. 198, 223–247.

Jung, S., Mezger, K., Masberg, P., Hoffer, E., Hoernes, S., 1998a. Petrology of an intrusion-related high-grade migmatite—implications for partial melting of metasedimentary rocks and leucosome-forming processes. J. Metamorph. Geol. 16, 425–445.

Jung, S., Mezger, K., Hoernes, S., 1998b. Petrology and geochemistry of post-collisional metaluminous A-type granites—a major and trace element and Nd–Sr–Pb–O-isotope study from the Proterozoic Damara Belt, Namibia. Lithos 45, 147–175.

Jung, S., Hoernes, S., Mezger, K., 2000. Geochronology and petrology of migmatites from the Proterozoic Damara Belt—importance of episodic fluid-present disequilibrium melting and consequences for granite petrology. Lithos 51, 153–179.

Jung, S., Mezger, K., Hoernes, S., 2002. Synorogenic melting of mafic lower crust: constraints from geochronology, petrology and Sr, Nd, Pb, O isotope geochemistry of quartz diorites (Damara orogen, Namibia). Contrib. Mineral. Petrol. 143, 551–566.

Jung, S., Hoernes, S., Mezger, K., 2003. Petrology of basement-dominated terranes: II. Contrasting isotopic (Sr, Nd, Pb, and O) signatures of basement-derived granites and constraints on the source region of granite (Damara orogen, Namibia). Chem. Geol. 199, 1–28.

Jung, S., Mezger, K., Hoernes, S., 2004. The role of crustal contamination and source composition in the petrogenesis of shear zone-related syenites (Damara belt, Namibia)—constraints from U–Pb geochronology and Nd–Sr–Pb–O isotope compositions. Contrib. Mineral. Petrol. 148, 104–121.

Jung, S., Hoernes, S., Hoffer, E., 2005. Petrogenesis of cogenetic nepheline and quartz syenites and granites (northern Damara orogen, Namibia)—enriched mantle vs. crustal contamination. J. Geol. 113, 651–672.

Kochar, N., 1990. Role of Malani anorogenic magmatism in the crustal evolution of the northwest Indian shield. In: McManus, M.N. (Ed.), Proterozoic Crustal and Metallogenic Evolution. Geol. Soc. and Geol. Surv. Namibia (abstracts), p. 43.

Kröner, A., 1982. Rb/Sr geochronology and tectonic evolution of the Pan-African Damara belt of Namibia, Southwestern Africa. Am. J. Sci. 282, 1471–1507.

Lechler, P.J., Desilets, M.O., 1987. A review of the use of loss on ignition as a measurement of total volatiles in whole rock analysis. Chem. Geol. 63, 341–344.

Litvinovsky, B.A., Zanvilevich, A.N., Wickham, S.M., Steele, I.M., 1999. Origin of syenitic magmas from anorogenic granitoid series: syenite–granite series from Transbaikalia. Petrology 7, 483–508.

Litvinovsky, B.A., Jahn, B.-M., Zanvilevich, A.N., Shadaev, M.G., 2002. Crystal fractionation in the petrogenesis of an alkali monzodiorite–syenite series: the Oshurkovo plutonic sheeted complex, Transbaikalia, Russia. Lithos 64, 97–130.

Lubala, R.T., Frick, C., Roders, J.H., Walraven, F., 1994. Petrogenesis of syenites and granites in the Schiel Alkaline complex, Northern Transvaal, South Africa. J. Geol. 102, 307–316.

Ludwig, K.R., 1991a. PBDAT: a computer program for processing Pb–U–Th isotope data. Version2.75. U.S. Geol. Surv. Open File Rep. 88–542.

Ludwig, K.R., 1991b. ISOPLOT: a plotting and regression program for radiogenic isotope data. Version 2.75. U.S. Geol. Surv. Open File Rep. 91–445.

Masberg, H.P., Hoffer, E., Hoernes, S., 1992. Microfabrics indicating granulite-facies metamorphism in the low-pressure central Damara Orogen, Namibia. Precambrian Res. 55, 243–257.

Mattinson, J.M., 1986. Geochronology of high-pressure–low temperature Franciscan metabasites. A new approach using the U–Pb system. Mem. Geol. Soc. Amer. 164, 95–105.

McDermott, F., Hawkesworth, C.J., 1990. Intracrustal recycling and upper-crustal evolution: a case study from the Pan-African Damara mobile belt, central Namibia. Chem. Geol. 83, 263–280.

McDermott, F., Harris, N.B.W., Hawkesworth, C.J., 1989. Crustal reworking in southern Africa: constraints from Sr–Nd isotope studies in Archaean to Pan-African rocks. Tectonophysics 161, 257–270.

Menzies, M., 1987. Alkaline rocks and their inclusions: a window on the earth's interior. In: Fitton, J.G., Upton, B.G. (Eds.), Alkaline igneous rocks. Geol. Soc. Spec. Publ., vol. 30, pp. 15–27.

Michard, A., Guriet, P., Soudant, M., Albarède, F., 1985. Nd isotopes in French Phanerozoic shales: external vs. internal aspects of crustal evolution. Geochim. Cosmochim. Acta 49, 601–610.

Miller, R.McG., 1983. The Pan-African Damara orogen of South West Africa/Namibia. Spec. Publ. - Geol. Soc. S. Afr. 11, 431–515.

Miller, R.McG., Burger, A.J., 1983. U–Pb zircon age of the early Damaran Naauwpoort Formation. Spec. Publ. - Geol. Soc. S. Afr. 11, 267–272.

Miller, C., Schuster, R., Klözli, U., Frank, W., Purtscheller, F., 1999. Post-collisional potassic and ultrapotassic magmatism in SW Tibet: geochemical and Sr–Nd–Pb–O isotopic constraints for mantle source characteristics and petrogenesis. J. Petrol. 40, 1399–1424.

Mingram, B., Trumbull, R.B., Littman, S., Gerstenberger, H., 2000. A petrogenetic study of anorogenic felsic magmatism in the Cretaceous Paresis ring complex, Namibia: evidence for mixing of crust and mantle-derived components. Lithos 54, 1–22.

Mitchell, R.H., Bergman, S.C., 1991. Petrology of Lamproites. Plenum press, New York.

Morse, S.A., 1970. Alkali feldspars with water at 5 kb pressure. J. Petrol. 11, 221–251.

Reiners, P.W., Nelson, B.K., Ghiorso, M.S., 1995. Assimilation of felsic crust by basaltic magma: thermal limits and extents of crustal contamination of mantle-derived magmas. Geology 23, 563–566.

Rollinson, H.R., 1993. Using Geochemical Data: Evaluation, Presentation, Interpretation. Longman, John Wylie and Sons, 352 pp.

Seth, B., Kröner, A., Mezger, K., Nemchin, A.A., Pidgeon, R.T., Okrusch, M., 1998. Archaean to Neoproterozoic magmatic events in the Kaoko belt of NW Namibia and their geodynamic significance. Precambrian Res. 92, 341–363.

Seth, B., Jung, S., Hoernes, S., 2002. Isotope constraints on the origin of Pan-African granitoid rocks in the Kaoko Belt, NW Namibia. S. Afr. J. Geol. 105, 179–192.

Smith, I.E.M., White, A.J.R., Cappell, B.W., Eggleton, R.A., 1988. Fractionation in a zoned monzonite pluton: Mount Dromedary, southeastern Australia. Geol. Mag. 125, 273–284.

Smith, D.R., Barnes, C., Shannon, W., Roback, R., James, E., 1997. Petrogenesis of Mid-Proterozoic granitic magmas: examples from central and western Texas. Precambrian Res. 85, 53–79.

Stacey, J.S., Kramers, J.D., 1975. Approximation of terrestrial lead isotope evolution by a two-stage model. Earth Planet. Sci. Lett. 26, 207–221.

Sun, S.-S., McDonough, W.F., 1989. Chemical and isotopic systematics of oceanic basalts: implications for mantle composition and processes. In: Saunders, A.D., Norry, M.J. (Eds.), Magmatism in the Ocean Basins. Geol. Soc. Spec. Publ., vol. 42, pp. 313–345.

Sutcliff, R.H., Smith, A.R., Doherty, W., Barnett, R.L., 1990. Mantle derivation of Archaean amphibole-bearing granitoids and associated mafic rocks: evidence from the Southern Superior Province, Canada. Contrib. Mineral. Petrol. 105, 255–274.

Taylor, S.R., McLennan, S.M., 1985. The Continental Crust: Its Composition and Evolution. Blackwell, London.

Tegtmeyer, A., Kröner, A., 1985. U–Pb zircon ages for granitoid gneisses in northern Namibia and their significance for Proterozoic crustal evolution of southwestern Africa. Precambrian Res. 28, 311–326.

Thirlwall, M.F., Burnard, P., 1990. Pb–Sr–Nd isotope and chemical study of the origin of undersaturated and oversaturated shoshonitic magmas from the Borralan pluton, Assynt, NW Scotland. J. Geol. Soc. (Lond.) 147, 259–269.

Thompson, R.N., Fowler, M.B., 1986. Subduction-related shoshonitic and ultrapotassic magmatism: a study of Siluro-Ordovician syenites from the Scottish caledonides. Contrib. Mineral. Petrol. 94, 507–522.

Zanvilevich, A.N., Litvinovsky, B.A., Wickham, S.M., Bea, F., 1995. Genesis of alkaline and peralkaline syenite–granite series, the Khartonovo pluton (Transbaikalia, Russia). J. Geol. 103, 127–145.

Zhao, J.-X., Shiraishi, K., Ellis, D.J., Sheraton, J.W., 1995. Geochemical and isotopic studies of syenites from the Yamato Mountains, East Antarctic: implications for the origin of syenitic magmas. Geochim. Cosmochim. Acta 59, 1363–1382.